

A comprehensive review and outlook of bifacial photovoltaic (bPV) technology

Wenbo Gu¹, Tao Ma^{1*}, Salman Ahmed¹, Yijie Zhang¹, Jinqing Peng²

¹*School of Mechanical Engineering, Shanghai Jiao Tong University, Shanghai, China*

²*College of Civil Engineering, Hunan University, Changsha, Hunan, China*

*Corresponding author: tao.ma@connect.polyu.hk Tel.: +86 21 3420 6056

Abstract

Bifacial photovoltaic (bPV) technology is regarded as a promising alternative, as it can generate more power than conventional mono-facial PV (mPV) technology by absorbing sunlight from both sides. However, technology review on bPV technology is quite limited. In addition, some challenges, such as complex mechanisms, non-uniform rear-side irradiance and other issues constrain the development of bPV technology. Therefore, it is necessary to present an overview on recent development of bPV technology from various perspectives and provide some potential directions for future research. In this study, an overview of bPV technology is demonstrated, including its working principle, comparison with traditional mPV technology and classification by cell type and backsheet material. Moreover, recent research and development on bPV technology from previous publications is discussed with respect to numerical modelling, software simulation, experimentation, economics, parameters involved, performance characterization and system applications. Finally, some future perspectives and potential approaches are proposed for future research and to make bPV technology

more cost-effective and competitive, since the current levelized cost of energy of bPV is only 2-6% lower than conventional mPV systems.

Keywords: Bifacial photovoltaic (bPV); Review and outlook; Modelling and experimental study; Performance characterization; Applications

1 Introduction

The Earth has long been considered as a planet that would face energy crisis, global warming and air pollution since the beginning of electrification era (Ma et al., 2018; Pan et al., 2020). Faced with these challenges, utilization of renewable energy resources has been proposed for a sustainable alternative, especially solar photovoltaic (PV) systems due to the abundance of solar energy (Chen et al., 2019). The global PV industry has expanded excessively in the past decade, with around 505 GW of global PV cumulative installation by 2018 (REN21). Future research will focus on system optimization and cost reduction associated with grid parity, which is specifically considered by China's 531 New Policy (Katsaounis et al., 2019; Liang et al., 2019).

Under these circumstances, the interest in crystalline silicon cells within the market and academic circles has shifted from mono-facial PV (mPV) technology to bifacial PV (bPV) technology, increasing from less than 10% in 2018 to 60% in 2029 as presented in Fig. 1 (VDMA, 2019).

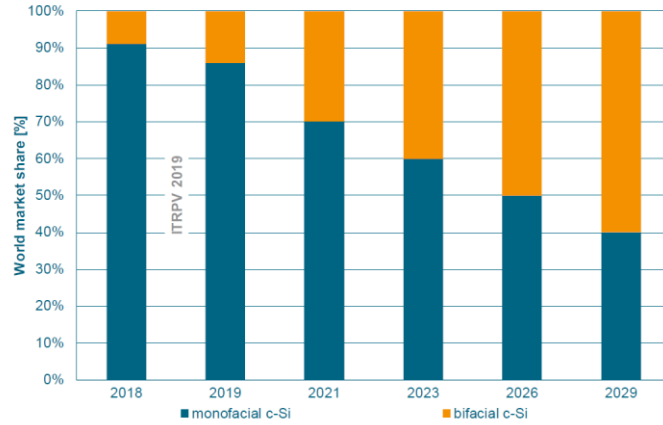


Fig. 1 The development trend of crystalline silicon (VDMA, 2019).

The bPV technology seems to be a novel concept, but the first work done on bPV technology can be traced back to a patent issued by Hiroshi in 1966 (Hiroshi, 1966). The first bifacial lab cell was fabricated and exhibited in 1977 (Luque et al., 1978), followed annually with few articles about high efficiency and real applications (Cuevas et al., 1982; Kasahara et al., 2003) as presented in Fig. 2.

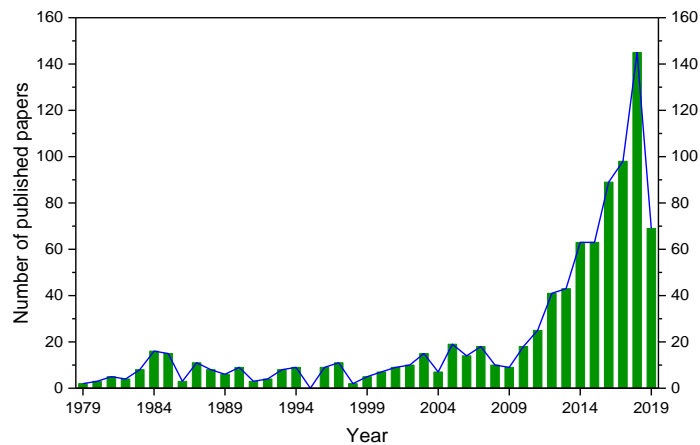


Fig. 2 Number of published papers about bPV technology from 1979 to Aug., 2019.

It can be seen that articles about bPV technology began increasing from 2009, as researchers started working on this novel technology on a global stage, especially from countries that were already major

players in the PV industry such as China, United States of America, Germany and Japan as shown in Fig. 3. Further details like mathematic models, were explored about bPV technology, particularly after 2009. However, these models were at times so simple that they could not accurately describe bPV characterizations and explain the complex relationships among sunlight, electricity and heat. In addition, some experimentations were undertaken but without long-term field evaluations. Technology review on bPV is quite limited and thus, it is necessary to present an overview on recent bPV development from various perspectives and provide some potential directions for future research.

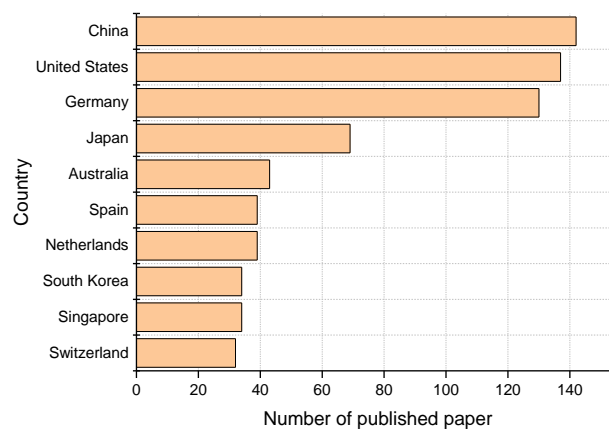


Fig. 3 Top 10 countries about bPV technology papers until Aug., 2019.

This paper, which is divided into 5 sections, presents a comprehensive review and outlook of the bPV technology, in order to help the researchers interested in this field to thoroughly understand this novel technology. Section 2 gives an overview of the bPV technology. Section 3 illustrates the performance of such systems with reference to mathematical models, computer simulations, experimental tests, economic factors, parametric analysis, testing methods and practical applications. Challenges faced

by bPV systems are presented in section 4, followed by some potential approaches and future perspectives. Finally, a brief summary of the study is given in section 5.

2 Overview of bPV technology

2.1 Principle of bPV

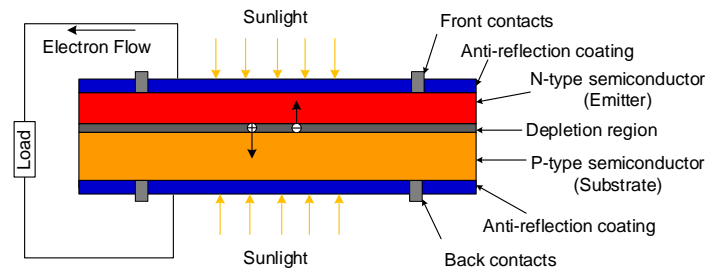


Fig. 4 Schematic of bPV technology.

Bifacial PV technology has a similar working principle as mPV, namely photoelectric effect. Compared to mPV, bPV cells add a layer of anti-reflection coating and back contacts instead of the back surface field (BSF) at the back side of PV cells. This is due to the property of absorbing sunlight from both sides as presented in Fig. 4. When solar cells are exposed to the sun, light transmits through the anti-reflection coatings from both sides of PV cells. The photon with higher energy than band gap passes a part of its energy to the electron as electron-hole pairs (Gu et al., 2019b). Carriers generating near the depletion region inside the semiconductor, are not recombined but to diffuse to the substrate and emitter. The carriers are then attracted by the internal electric field, causing electrons to flow into the N-type semiconductor and holes flow into the P-type semiconductor. As a result, an electromotive

force generates between the front and back contacts. Electrons flow through the external load once both sides of the PV cells are connected.

2.2 Technology of bPV vs mPV

As a novel technology, the cell structure and appearance of bPV cells have many differences from mPV cells as presented in Fig. 5. Due to the property of absorbing sunlight from both sides, this special structure contributes to 5-30% more power output, and 2-6% lower levelized cost of energy (LCOE) (Patel et al., 2019), despite the complex manufacturing, installation and design with the risk for more shade of back side. In addition, conventional organic backsheets suffer from pulverization, because of the exposure to ultraviolet rays from the ground, and experience functional failure due to the gaps and intrusions of water vapor (Barbato et al., 2017; Carolus et al., 2019). The glass-glass structure of the bPV modules contributes to a lower cleaning frequency (Bhaduri and Kottantharayil, 2019) and longer lifetime, than mPV modules that have the traditional glass-organic backsheet structure (Guo et al., 2013), because of lower cell temperature (Guerrero-Lemus et al., 2016; Lamers et al., 2018) and stronger endurance to unfavorable environment (Sun et al., 2018). Furthermore, bPV modules can be used in wider applications, such as noise barriers (Faturrochman et al., 2018) and building facades (Soria et al., 2016), due to insensitivity towards orientation and inclination.

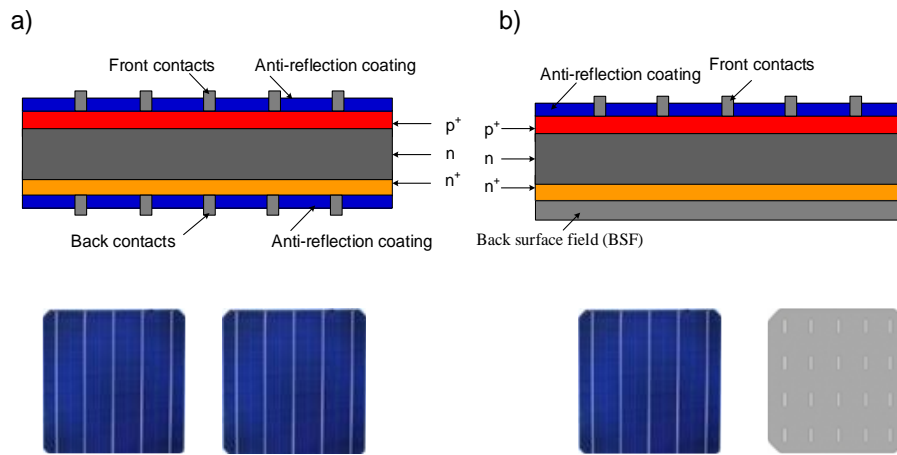


Fig. 5 Different cell structures and appearance: a) bPV; b) mPV (Gu et al., 2020).

2.3 Bifacial PV modules categories

2.3.1 Various types of bPV

With the increasing demand of highly efficient PV cells, various bifacial modules based on bPV technology with different manufacturing processes are available in the PV market. These include passivated emitter rear contact (PERC), passivated emitter rear locally-diffused (PERL), passivated emitter rear totally diffused (PERT), heterojunction with intrinsic thin-layer (HIT), interdigitated back contact (IBC) and double-sided buried contact solar cell (DSBCSC) (Liang et al., 2019). A basic view of each module can be seen in Fig. 6. The differences of structure results in various bifaciality coefficient ranges for these PV cells: 70-80% (PERC, IBC and DSBCSC); 80-85% (PERL and PERT); 95-100% (HIT), indicating that HIT can generate more power output under the same conditions.

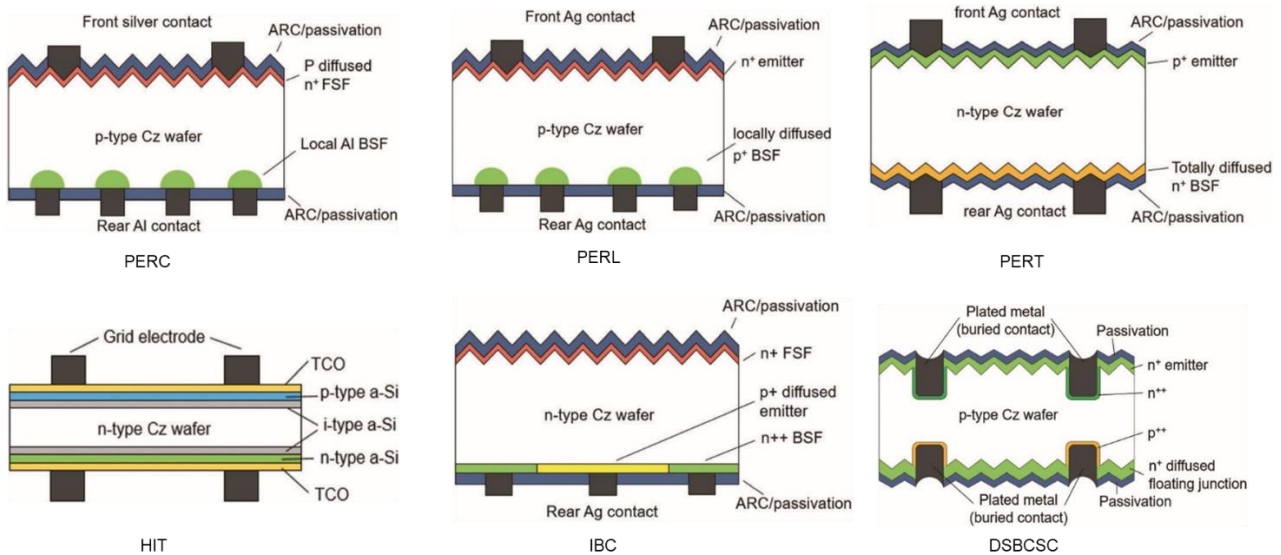


Fig. 6 Various bPV structure (Liang et al., 2019).

2.3.2 Backsheet materials

Backsheet materials like glass and transparent organic material, can also be used as a standard to categorize bifacial modules. Bifacial PV modules with glass instead of transparent organic material, can stand unfavorable environmental conditions for longer durations due to the glass protection (Guo et al., 2013; Sun et al., 2018). Furthermore, these types of PV modules have durable waterproof performance to strengthen the anti-potential induced degradation (anti-PID) (Barbato et al., 2017; Carolus et al., 2019; Sporleder et al., 2019). Bifacial PV modules with transparent organic materials also have many advantages, such as having a lower weight, stronger anti-soiling ability and lower cell-to-module current loss, which contributes to a notable market share for such type of bPV systems. It is observed that bPV modules are highly recommended in developed countries with high labor cost, because of the lower price for balance of system and operation expense (Saw et al., 2017; Singh et al., 2015).

3 Comprehensive review on bPV technology

In this section, a detailed review of bPV technology in past literature is done with respect to mathematical modelling, software simulation, experimental test, economic issues, various parameters analysis, testing method and practical applications.

3.1 Mathematical modelling of bPV modules

To estimate the performance of a bPV modules, it is vital to develop some mathematical models in the form of coupled models or empirical formulae (Gu et al., 2019a).

3.1.1 Coupled models

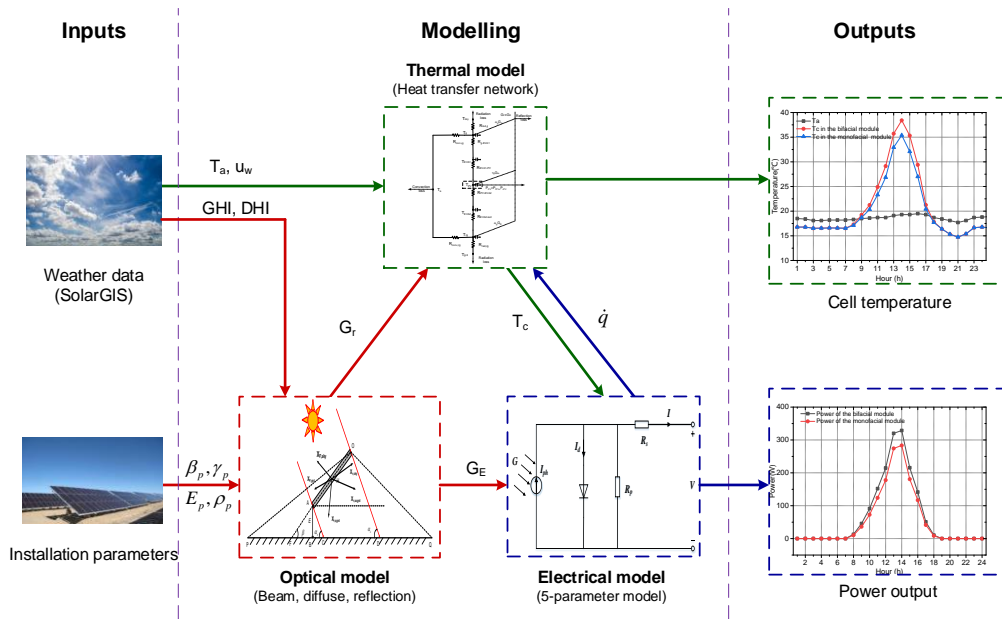


Fig. 7 Schematic diagram of the coupling models (Gu et al., 2020).

For the coupled model technique, three sub models are included, namely the optimal model, electrical model and thermal model, with their coupling schematic diagram presented in Fig. 7 (Gu et al., 2020).

Onsite weather parameters (GHI and DHI) and installation parameters (tilt angle β_p , azimuth angle

γ_p , elevation E_p and albedo ρ_p) are the inputs for the optical model. Based on the optical model, the equivalent irradiance G_E and received irradiance G_r can be easily calculated. Based on the thermal model, cell temperature T_c can be obtained, once the weather data (ambient temperature T_a and wind velocity u_w) along with the received irradiance and internal heat source \dot{q} (unabsorbed solar energy) is imported into the thermal model. Combined together, the outputs of the optical model and thermal model are fed as input to the electrical model, and lastly the module power output can be obtained (Sun et al., 2018). It is noted that a closed loop exists between the electrical and thermal models, indicating the coupled relationship between electricity and heat.

3.1.1.1 Optical modelling

A bPV module can absorb part of the sunlight to generate electricity with various optical losses. These optical losses occur at different interfaces of both sides, including reflection loss, absorption loss and transmittance loss (Saw et al., 2017) as presented in Fig. 8. Therefore, it is significant to appropriately obtain the irradiances of the bPV module from front and rear sides.

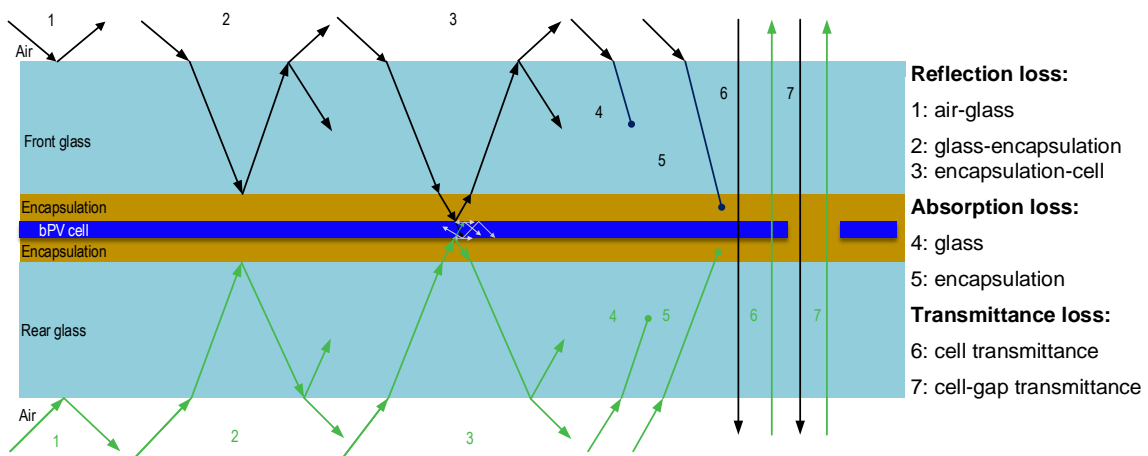


Fig. 8 Optical losses for a typical bPV module.

3.1.1.1.1 Front-side irradiance

The tilted front-side global irradiance G_F can be obtained as Eq. (1):

$$G_F = G_b^F + G_d^F + G_r^F = (GHI - DHI) \cdot R_b^F + G_d^F + GHI \cdot \rho_p \cdot \frac{1 - \cos \beta_p}{2} \quad (1)$$

where the superscript ‘F’ refers to front side, G_b , G_d and G_r are three parts of the global tilted irradiance, namely beam, diffusion and reflection, GHI (DHI) is the global horizontal irradiance (diffuse horizontal irradiance), obtained from some meteorological data companies, such as SolarGIS (Solargis) or estimated simply from clear sky model (Stein et al., 2012), β_p is the tilt angle of the PV panel, ρ_p is the albedo of the ground, and R_b^F is the ratio of front tilted irradiance and horizontal irradiance (Gu et al., 2020).

Diffuse irradiance is more complicated than beam and reflected irradiances and it has attracted researchers to work on models, such as the Liu and Jordan model, HDKR model and Perez model.

(a) Liu and Jordan model

Liu and Jordan model (Liu and Jordan, 1963) is a represent of the isotropic model, which is defined as Eq. (2):

$$G_d^F = DHI \cdot \left(\frac{1 + \cos \beta_p}{2} \right) \quad (2)$$

(b) HDKR model

Hay, Davies, Klucher and Reindl put forward their equations to improve the isotropic model, respectively, which were combined as HDKR model as presented in Eq. (3) (Duffie et al., 2006):

$$G_d^F = DHI \cdot \frac{(GHI - DHI)}{G_0} \cdot R_b^F + DHI \cdot \left(1 - \frac{(GHI - DHI)}{G_0}\right) \left(\frac{1 + \cos \beta_p}{2}\right) \left[1 + \sqrt{\frac{(GHI - DHI)}{GHI}} \sin^3\left(\frac{\beta_p}{2}\right)\right] \quad (3)$$

where G_0 is the global irradiance outside the atmosphere.

(c) Perez model

Perez et al. (Perez et al., 1986) proposed a so-called Perez model to estimate the tilted diffuse irradiance, consisting of horizontal brightening, circumsolar diffuse and sky isotropic diffuse irradiances as presented in Eq. (4):

$$G_d^F = DHI \cdot (1 - F_1) \left(\frac{1 + \cos \beta_p}{2}\right) + F_1 \frac{a}{b} + F_2 \sin \beta_p \quad (4)$$

where a and b represent the coefficients considering the effect of circumsolar incident angle on the tilted and horizontal panels on the diffuse irradiance, F_1 and F_2 present the conditions of circumsolar brightness and horizontal brightness (Perez et al., 1986).

In all, isotropic models are quite easy to calculate the related parameters, but not as accurate as those anisotropic models, especially Perez model under most conditions.

3.1.1.1.2 Rear-side irradiance

For rear-side irradiance modelling, there are two common methods to achieve the goal, namely view factor model and ray tracing, which would be introduced in detail.

(a) View factor model

View factor is a rather important concept in calculation of rear-side irradiance, which is expressed as Eq. (5) (Yusufoglu et al., 2015), and the schematic of view factor is presented in Fig. 9 (Yusufoglu et al., 2014).

$$X_{1,2} = \frac{1}{A_1} \int_{A_1} \int_{A_2} \frac{\cos \theta_1 \cos \theta_2 dA_2 dA_1}{\pi S^2} \quad (5)$$

where $X_{1,2}$ is the view factor of face 1 to face 2, A_1 and A_2 are the areas of face 1 and face 2, dA_1 and dA_2 are the areas of micro-element face 1 and micro-element face 2, θ_1 and θ_2 are the angles between the path and the normal vector of face 1 and face 2, and S is the distance between the center of micro-element face 1 and micro-element face 2.

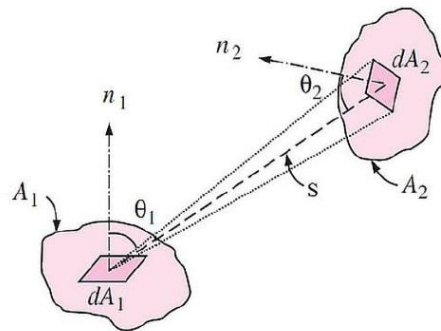


Fig. 9 Definition of view factor of $X_{1,2}$ (Yusufoglu et al., 2014).

For a specific bPV module with a height of H_p , elevation of E_p and tilt angle of β_p , there are three view factors for rear panel, namely $X_{R,sky}$, $X_{R,sgrd}$, and $X_{R,usgrd}$ as presented in Fig. 10.

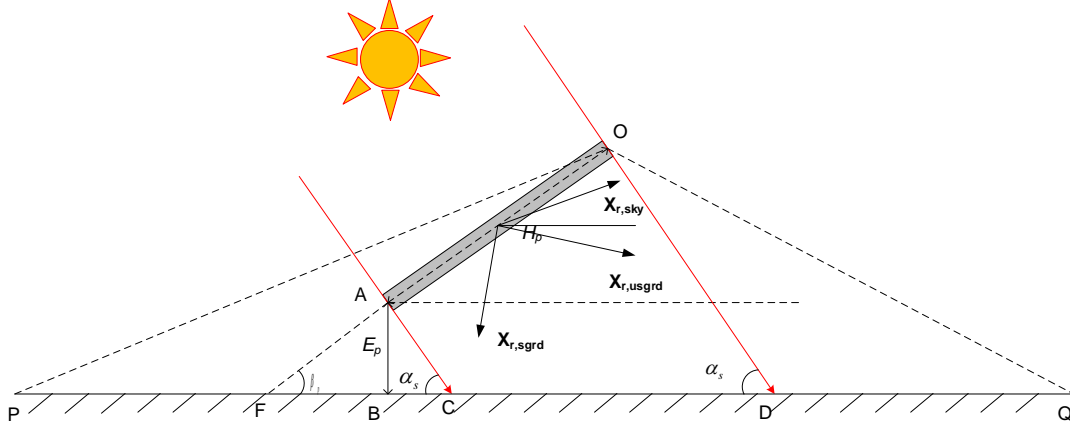


Fig. 10 Schematic of a PV module's view factor (Gu et al., 2020).

Under the case, the rear-side irradiance can be calculated from Eq. (6).

$$G_R = G_b^R + G_d^R + G_r^R = (GHI - DHI) \cdot R_b^R + DHI \cdot X_{R,sky} + GHI \cdot \rho_p \cdot X_{R,usgrd} + DHI \cdot \rho_p \cdot X_{R,sgrd} \quad (6)$$

where the superscript 'R' refers to rear side, R_b^R is the ratio of rear tilted irradiance and horizontal irradiance, $X_{R,sky}$ is the view factor of rear panel to sky, $X_{R,usgrd}$ is the view factor of rear panel to unshaded ground, and $X_{R,sgrd}$ is the view factor of rear panel to shaded ground. More details can be obtained in the literature (Appelbaum, 2018; Sönmez et al., 2019).

(b) Ray tracing model

Besides view factor model, ray tracing is another approximate tool incorporated in some software, such as RADIANCE (LBNL, 1990s), packages of Trace Pro (LRC, 2020) and COMSOL (Comsol, 2014), to predict the irradiance level of PV panel in a simpler way. After inputting the geometry

structure, materials properties, time and location into such software, we get spectral radiance, irradiance distribution, and glare indices as outputs in different forms (color images, numerical values and contour plots). Fig. 11 presents an example about front- and rear-side irradiances at a sunny noontime by RADIANCE software, in which front- and rear-side irradiance reaches 844 W/m^2 and $80\text{-}90 \text{ W/m}^2$, respectively (Deline et al., 2016).

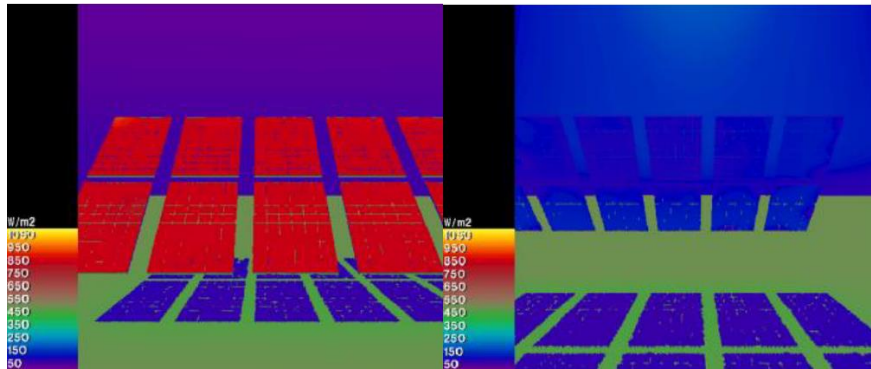


Fig. 11 Front- and rear-side irradiance simulated by RADIANCE (Deline et al., 2016).

As for the accuracy, the rear-side irradiances from view factor model, RADIANCE software and measurement are compared in Fig. 12. It can be clearly seen that the results with the view factor model is in better agreement with the measured than RADIANCE software. However, with the help of software, this method is capable of obtaining more details than view factor model, for example the gaps between cell to cell in a module and equipment rack. As a whole, the simulation results of rear irradiance by RADIANCE in the literature are acceptable under most cases (Deline et al., 2016), with normalized root mean square deviation (NRMSD) at $4\text{-}16\%$ (Asgharzadeh et al., 2018).

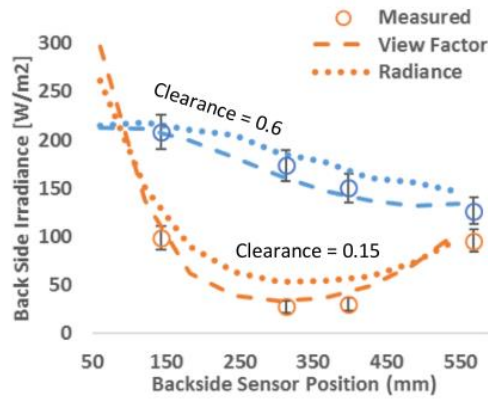


Fig. 12 Comparison of results from view factor model and RADIANCE software (Pelaez et al., 2019).

3.1.1.2 Electrical model

When it comes to the electrical performance of bPV technology, it is always associated with the concept of bifacial gain to show the advantage of bPV technology, as expressed in Eq. (7) (Cuevas et al., 1982; Sun et al., 2018):

$$\text{Bifacial gain (\%)} = (Y_{bPV} - Y_{mPV}) / Y_{mPV} \times 100 \quad (7)$$

where Y_{bPV} and Y_{mPV} refers to electricity yields of bPV and mPV modules during the test period, respectively.

It can be seen from Eq. (7) that it is rather significant to obtain the values of electricity production for the value of bifacial gain. Therefore, two practical methods, namely a single-point power model and equivalent circuit model, are introduced in this section to obtain the power output of bPV and mPV modules accordingly.

3.1.1.2.1 A single-point power model

The easiest electrical model is a single-point power model, which is expressed as Eq. (8) (Sun et al., 2018).

$$P_{PV} = G_F A \times \eta_F + G_R A \times \eta_R \quad (8)$$

where A is the area of the PV module, η_F and η_R are the electricity efficiency of the front and rear PV panel and can be calculated from Eq. (9) and (10), respectively.

$$\eta_F = \eta_{F,ref} [1 - \beta_{ref} (T_c - T_{c,ref})] \quad (9)$$

$$\eta_R = \eta_{R,ref} [1 - \beta_{ref} (T_c - T_{c,ref})] \quad (10)$$

where β_{ref} is the temperature coefficient of the bPV modules, $T_{c,ref}$ is the cell temperature under standard test conditions (STC), T_c is the cell temperature under non-STC, $\eta_{F,ref}$ and $\eta_{R,ref}$ is the electricity efficiency of the front and rear PV panel under STC, which can be obtained from the manufacturers.

It can be observed that the power output of a mPV module can be easily calculated ($G_R = 0$). However, it is hard to repeat this for a bPV module, since the rear-side irradiance is not constant and the dependence on various conditions when the front side is under STC. Therefore, usually manufacturers provide the bifacial power output with a linear addition of the front-side power under STC and a series of particular rear-side irradiances.

3.1.1.2.2 Equivalent circuit model

As mentioned above, it is easy to calculate the power output according to the above approach.

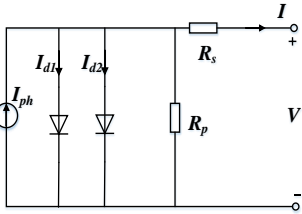
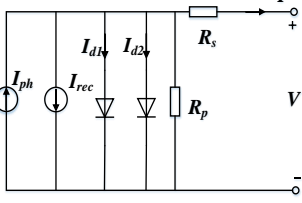
However, it can only get some results with low accuracy, thus deterring the popularity of the approach.

Therefore, a highly accurate equivalent circuit model is usually used in academic circles. Table 1

summarizes various equivalent circuit models according to the number of diodes and parameters.

Table 1 Summary of various equivalent circuit models.

Group	Model	Parameters	References	Equivalent circuit
One-diode	4-parameter model	I_{ph}, I_0, R_s, n	Tossa et al. (Tossa et al., 2014)	
	5-parameter model	I_{ph}, I_0, R_s, R_p, n	Mermoud et al. (Mermoud and Wittmer, 2018); Gu et al. (Gu et al., 2020)	
	6-parameter model	$I_{ph}, I_0, R_s, R_p, n, I_{rec}$	Merten et al. (Merten and Andreu, 1998; Merten et al., 1998; Merten et al., 2012); Piccoli (Piccoli, 2017)	
Two-diode	6-parameter model	$I_{ph}, I_{01}, I_{02}, R_s, n_1, n_2$	Dobos et al. (Dobos, 2012); Tossa et al. (Tossa et al., 2014)	

	7-parameter model	$I_{ph}, I_{01}, I_{02}, R_s,$ R_p, n_1, n_2	Yordanov et al. (Yordanov et al., 2012); Yusufoglu et al. (Yusufoglu et al., 2015)	
	8-parameter model	$I_{ph}, I_{01}, I_{02}, R_s,$ R_p, n_1, n_2, I_{rec}	Merten et al. (Merten et al., 2008); Tossa et al. (Tossa et al., 2014)	

Based on the model listed in Table 1, the characteristic curves of mPV modules and front side of bPV modules under STC can be calculated as shown in Fig. 13. Then, the characteristic curves of PV modules under non-STC can also be obtained with some parameter conversion (Bai et al., 2014; Humada et al., 2016). The bPV power output can still be calculated if the rear-side irradiance is converted into the front-side irradiance with the concept of equivalent irradiance, which will be further discussed in section 3.6.1.

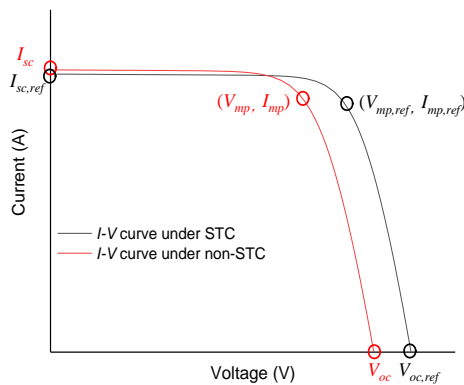


Fig. 13 The characteristic curves and parameters.

Besides, Shoukry et al. (Shoukry et al., 2016) employed Eq. (11)- (13) to calculate the power output of the bPV module.

$$I_{sc,b} = I_{sc,f} + I_{sc,r} \quad (11)$$

$$V_{oc,b} = V_{oc,f} + (V_{oc,r} - V_{oc,f} \ln((I_{sc,r} + I_{sc,f}) / I_{sc,f})) / \ln(I_{sc,r} / I_{sc,f}) \quad (12)$$

where the subscript 'b' refers to the bPV module, 'f' refers to front side, and 'r' refers to rear side.

$$P_{mpp} = FFV_{oc}I_{sc}(1 + \alpha_{mpp}(T - 25)) \quad (13)$$

where α_{mpp} is the temperature coefficient of the module at maximum power point (MPP), P_{mpp} is the power output at MPP, T is cell temperature in °C, and FF is fill factor.

3.1.1.3 Thermal model

Thermal models with different formulas in order to find out the bPV cell temperature. This section discusses the different models that are available.

(a) Sandia model

In Sandia model, cell temperature can then be obtained when the module temperature is estimated firstly as presented in Eq. (14)- (15) (Sandia; Sandia):

$$T_m = G \cdot (e^{a+b \cdot WS}) + T_a \quad (14)$$

$$T_c = T_m + \frac{G}{G_0} \Delta T \quad (15)$$

where WS is wind speed, a and b are parameters depending on the module construction and materials as well as on the mounting configuration, G_0 is a reference irradiance (1000 W/m²), and ΔT is a

temperature difference parameter, which defines the temperature difference between the module and cell temperature.

(b) NOCT model

Normal operating cell temperature (NOCT) model is employed to calculate the cell temperature of the bPV module by Yusufoglu et al. (Yusufoglu et al., 2015) and Shoukry et al. (Shoukry et al., 2016).

In their models, the T_{NOCT} is 2°C higher than that for estimating the mPV cell temperature.

$$T_c = T_a + \frac{T_{NOCT} - 20}{800} G \quad (16)$$

where T_a is the ambient temperature, T_{NOCT} is the nominal operating cell temperature in °C which is usually provided by the manufacturer for mPV, and G is the sum of irradiance on the both sides.

(c) PVsyst

The performance of bPV modules can be estimated by PVsyst software in newer versions, in which the thermal model based on Faiman model (Faiman, 2008) is employed as Eq. (17).

$$T_c = T_a + \frac{\alpha G(1-\eta)}{U_0 + U_1 \times WS} \quad (17)$$

where α and η is absorption and electricity efficiency of the bPV module, respectively, U_0 is the constant heat transfer component (25 W/m²K), and U_1 is the convective heat transfer component (1.2 W/m³sK).

(d) Calculation based on energy balance

To calculate the cell temperature based on energy balance, it is necessary to acquire the energy flows of bPV system, as presented in Fig. 14. It can be seen that sunlight is the input for the entire system. A portion of sunlight at the front is absorbed by glass, while the rest is transmitted through the front glass and absorbed by bPV cells. The solar path in rear-side PV panel is similar to the front side. The bPV cells absorb the sunlight from both sides simultaneously to generate electricity because of photoelectric effect. Various losses in the cell (transmission loss and thermalization loss) are totally treated as heat, which is then conducted to the front and rear glasses, and finally dissipated by convection and radiation.

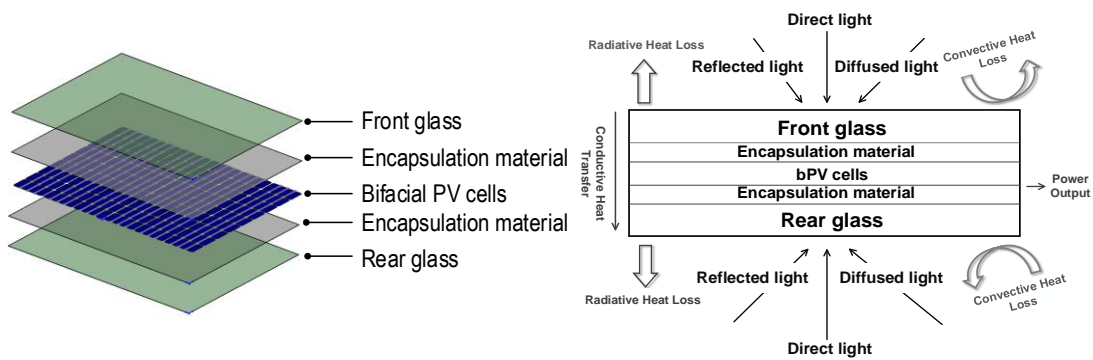


Fig. 14 Structure and energy flows for the bPV module.

Once the energy flows in the bPV module are considered accurately, various losses such as radiative loss and convective loss can be calculated (Abotaleb and Abdallah, 2018). Later the cell temperature of bPV modules can be obtained according to energy conservation.

3.1.2 Empirical formulae

Besides coupled models, the method of using empirical formulae can still be used to get some quick results, although its accuracy might be compromised.

(a) Kutzer model

The effects of albedo, bifaciality, row-to-row distance and height on the additional bifacial energy gain are taken into consideration in the Kutzer model (Kutzer et al., 2016) as presented in Eq. (18).

$$BG_E(\%) = \alpha \times \text{Bifaciality} \times 0.95 \times \left[0.317 \left(1 - \frac{1}{\sqrt{r}} \right) \left(1 - e^{-\frac{8.691h}{r}} \right) + 0.125 \left(1 - \frac{1}{r^4} \right) \right] \quad (18)$$

where BG_E is additional bifacial energy gain, r is the normalized row spacing ($r = R/CW$, R is the row spacing distance, CW is the PV collector width) and h is the normalized clearance height of the PV panel ($h = H_p/CW$, H_p is the clearance height of the PV panel).

(b) Castillo model

Some experimental tests were performed by Castillo et al. (Castillo-Aguilella and Hauser, 2016), and an empirical best-fit model based on the experimental results is defined to predict the annual energy yield of bifacial modules as presented in Eq. (19).

$$BG_E[\%] = 0.317 \times \beta_p[^\circ] + 12.145 \times H_p[\text{m}] + 0.1414 \times \alpha[\%] \quad (19)$$

where α is the albedo of the local ground, β_p is the tilt angle of the bPV panel in degrees for a range of 7.5- 35 degrees. There are certain limitations to estimate the bPV performance using this empirical model under some complex conditions instead of theory analysis.

It can be observed from Eq. (18)- (19) that BG_E is always proportional to H_p in the Castillo model.

While the growth rate reduces as H_p increases in Kutzer model although both of BG_E in these two

models increase with a rise of H_p . In all, these empirical formulae are only used to get some rough results to guide the design of bPV system, which cannot replace a coupled model in practice to estimate the bPV performance with high accuracy.

3.2 Software simulation of bPV

The performance of bPV especially electrical performance, can be obtained accurately from coupled models described above, although it is complicated and unnecessary for some beginners to understand these relationships. Under such circumstances, simulation software including some open source software and commercial software may be a good choice because of their simplification, such as bifacialvf (NREL), PV_Lib Toolbox (Sandia) System advisor model (SAM) (NREL, 2018b) and PVSyst software (NREL, 2018a). In this section, SAM and PVSyst is introduced briefly as a representative of open source software and commercial software, respectively.

3.2.1 SAM

SAM is also developed by National Renewable Energy Laboratory (NREL) to model techno-economic performance of various renewable energy system, including bPV systems (NREL, 2018b).

Fig. 15 presents the interface of SAM for bifacial system design. It can be observed that bPV performance is based on the characteristic parameters of the front side at reference conditions. Bifacial specifications, namely transmission fraction, bifaciality and ground clearance height are the variables to be determined by designers. It should be noted that two methods are selective to make temperature corrections, namely NOCT method and heat transfer method as aforementioned.

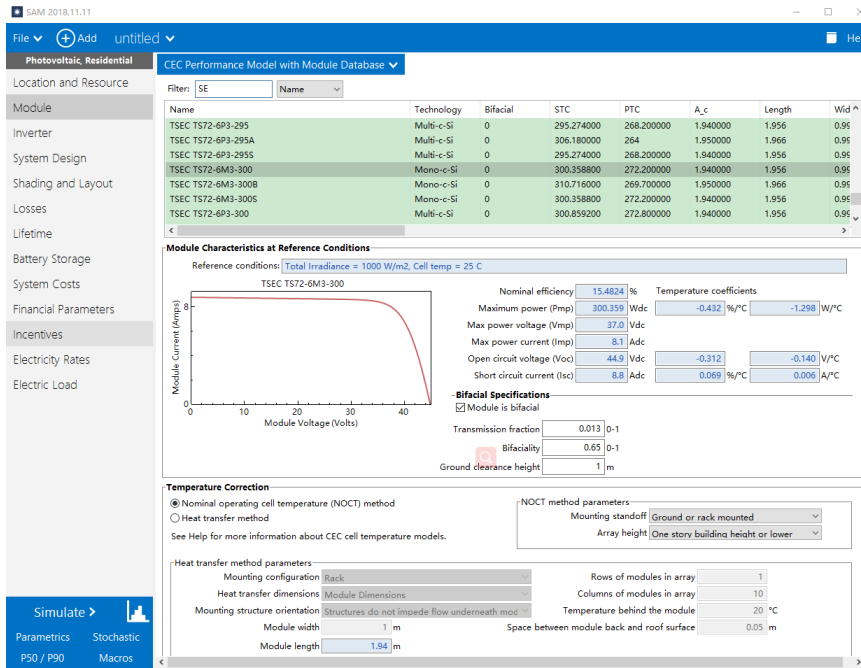


Fig. 15 Software interface of bifacial system design for SAM (NREL, 2018b).

3.2.2 PVsyst

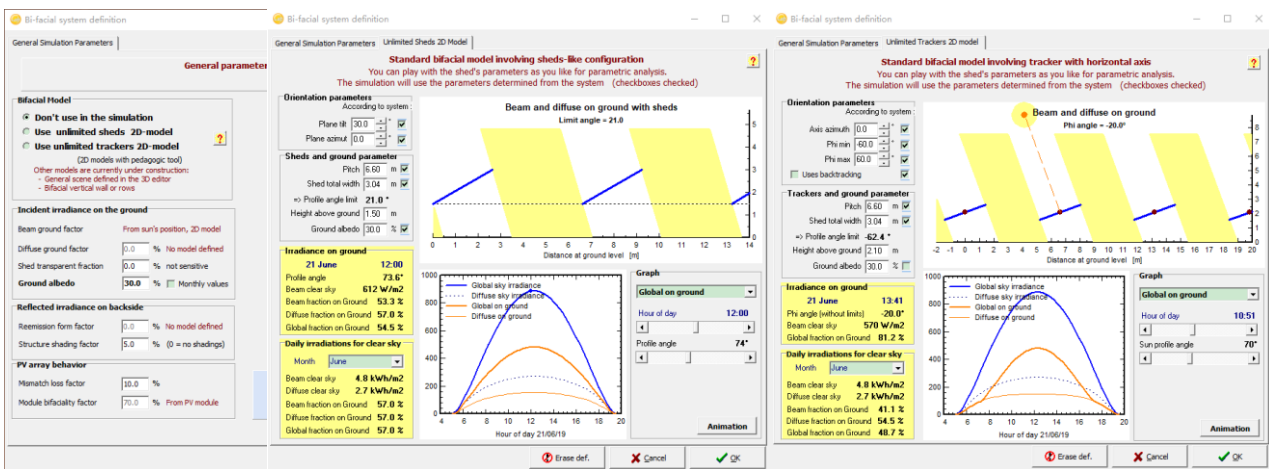


Fig. 16 Software interface of bifacial system design for PVsyst (NREL, 2018a).

PVsyst software is widely-used for designers in PV simulation field. Bifacial model is also introduced into this typical software under some assumptions. Some main assumptions include having an equal row distance and a very long length PV string without considering edge effect. Two bifacial models are provided to estimate the bPV performance, including unlimited sheds 2D-model and unlimited

trackers 2D-model as presented in Fig. 16. The difference between these two bifacial models is that the former is for fixed bPV arrays while the latter is for horizontal single-axis tracking bPV arrays.

3.3 Experimental study and real system operation performance

Besides numerical simulations, some experiments were carried out not only to validate their models, but also obtain the performance of bPV modules under real operation conditions.

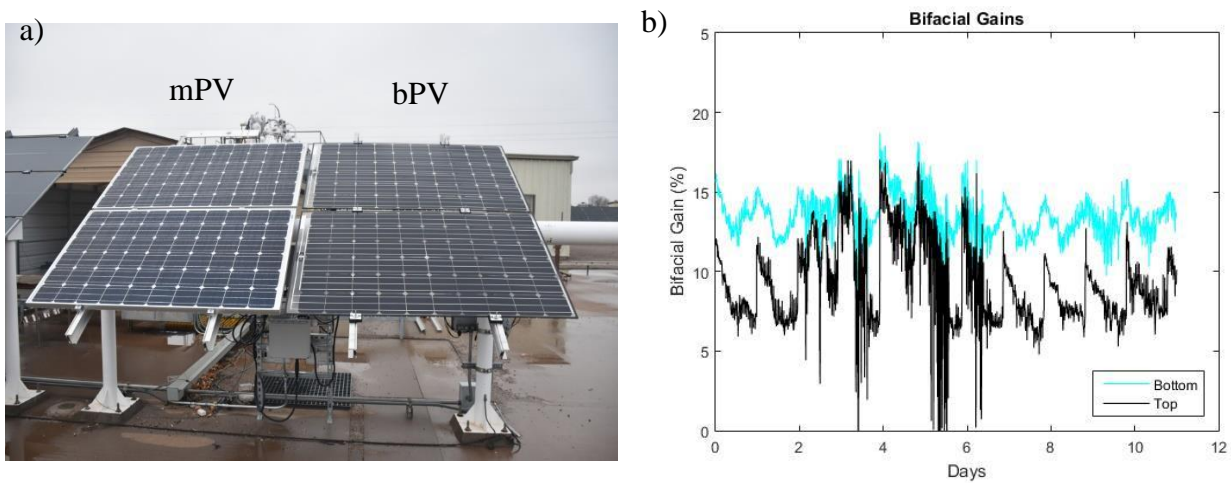


Fig. 17 A field example of bPV performance by Sandia National Laboratories: a) experimental setup; b) bifacial gain as experimental results (Sandia).

In a field example (Sandia), two mPV and two bPV modules facing south were installed at a tilt angle of 35° (Fig. 17 (a)), and bifacial gains of the top and bottom rows were calculated. Bifacial gains of the two rows fluctuated from about 7% to 16% (Fig. 17 (b)). The bifacial gain of bottom row was higher than that of the top row because of shorter distance from the bright area for the bottom modules. For one clear day, the bifacial gain was still fluctuating and the value in the morning was the highest

of the whole day due to the relative position of these two modules: the sunlight in the morning hits the ground directly beneath the bPV module while the shadow was projected under the mPV module.

Similar experiments for estimating the bPV performance were also conducted by other research groups. For example, the annual bifacial gain reached 5% at south orientation, with 40° tilt and an albedo of 0.05 (Molin et al., 2018). Many factors influence the bifacial gain. For exploring the effects of various factors, 7 different test conditions were employed by Castillo et al. (Castillo-Aguilella and Hauser, 2016) to calculate the annual average bifacial gain in field, varying from 12.3% - 30% and a best-fit relationship between bifacial gain and various factors was developed. Bifacial gains of different background were measured by experiments: 7.6% on grass, 15% on sand and 29.2% on snow (Wei et al., 2016). To obtain higher bifacial gains, some optimized system designs by experiments were proposed, such as higher albedo, fewer backside obstructions and less ground shading beneath the array (Stein et al., 2017). Through experiments, Rabanal-Arabach et al. (Rabanal-Arabach and Schneider, 2016) found that albedo and ambient temperature were the main module temperature drivers. Reduction of infrared reflection and increasing visible wavelength reflection were suggested to improve the bPV performance and reliability, especially in desert areas. Some experiments validated that micro inverter is much more proper than string inverter, with a higher index of bifacial gain (Stein et al., 2017; Yu et al., 2016).

3.4 Economic issues of bPV

LCOE is a significant concept in PV economic estimation, as it reveals if the grid parity of electricity produced by PV can be realized (Saw et al., 2017), and is defined as (Branker et al., 2011):

$$LCOE = \frac{\sum_{n=1}^N \frac{C_n}{(1+r)^n}}{\sum_{n=1}^N \frac{E_n}{(1+r)^n}} = \frac{\sum_{n=1}^N \frac{I_n + O_n + M_n + F_n}{(1+r)^n}}{\sum_{n=1}^N \frac{S_n(1-d)^n}{(1+r)^n}} \quad (20)$$

where N is the lifetime of a PV project, r is discount rate, d is degradation rate, E_n and S_n are actual and rated electricity production in year n , and net costs C_n in year n contains initial investment I_n , operation costs O_n , maintenance costs M_n , and interest expenditures F_n .

It is well acknowledged that the differences of LCOE between bPV and mPV are mainly associated with two factors, namely energy production and initial cost especially the cost of manufacturing. Energy production of mPV and bPV is affected by various other factors and will be discussed in section 3.5. The mPV and bPV manufacturing cost is demonstrated in Fig. 18. It can be seen that the difference in manufacturing cost between various bPV technology and mPV reaches 0-15.6% depending on manufacturing technology. It is noted that the cost of bifaical PERC technology is the same as mPV. The manufacture cost will reduce constantly as bPV technology develops further, ultimately reducing the LCOE.

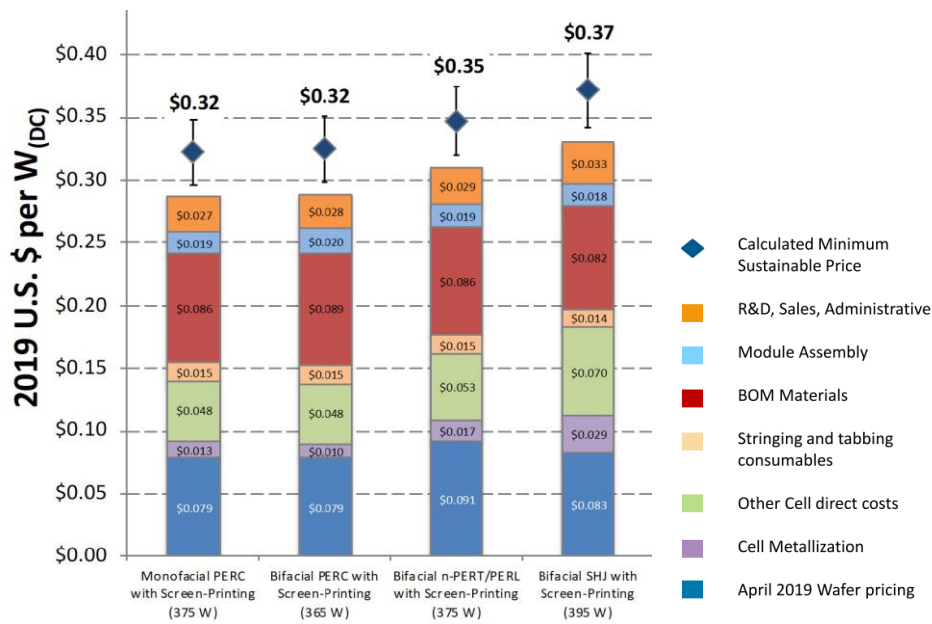


Fig. 18 Manufacture cost of mPV and various bPV modules (Deline et al., 2019).

The research on economic issues of bPV, especially LCOE will be a hot topic in the future, although there are just few studies on LCOE of bPV as of now. It is well known that the use of bifacial technology on PV cells can contribute to lower the LCOE than conventional mPV cells in real applications (Fertig et al., 2016) up to 2- 6% (Patel et al., 2019), but the value of LCOE is in fact affected by various factors such as installation and location. Tillmann et al. (Tillmann et al., 2020) obtained a function of minimum LCOE with row distance and tilted angle for various land consumption costs based on Bayesian optimization algorithm, which can offer some suggestions on the reduction of LCOE up to 23%. Range of LCOE around the world is from 3.29-14.43 USD cents/kWh, which mainly depends on the ground albedo and solar irradiance. The specific value of LCOE for numerous cities can be found in Ref. (Rodríguez-Gallegos et al., 2018). The concept of LCOE can also be employed to determine which one is more cost-effective for mPV and bPV modules with any module orientation (AMO) or vertical module orientation (VMO). The results obtained by

Rodríguez-Gallegos et al. (Rodríguez-Gallegos et al., 2018) from global perspective show that for latitudes higher than 40° , bifacial AMO modules are always more cost-effective than mono-facial AMO systems regardless of ground albedo. However, this trend is reversed for latitudes below 40° unless the albedo value is higher than a minimum value of about 0.12- 0.30. For the comparison between mono-facial AMO and bifacial VMO, the latter is more cost-effective under two conditions: a) latitudes are higher than 65° ; b) the albedo is higher than a minimum value, 0.29-0.57 although latitudes are below 65° .

3.5 Various impact factors of bPV module performance

As Fig. 19 shows, the performance of bPV modules is governed by various factors including three aspects. These include bifacial technology, local meteorological and geographical information (sun position, soiling, shading and diffuse coefficient and ground albedo) and installation information (orientation, tilt angle, row distance and module elevation) (Van Aken and Carr, 2014). In this subsection, some important factors will be discussed in detail.

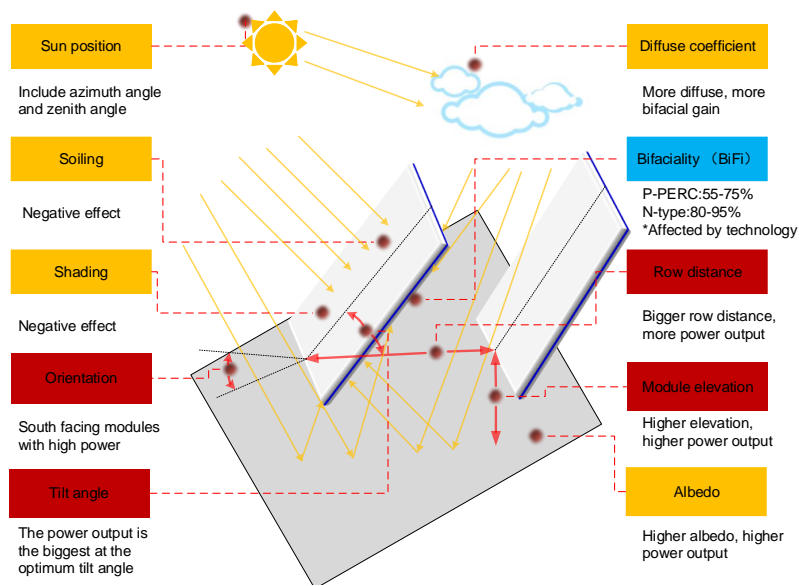


Fig. 19 Various factors affecting the performance of the bPV modules.

3.5.1 Albedo

Rear irradiance is largely dependent on the reflection of ground. High albedo contributes to high rear irradiance, resulting in high bifacial energy yield (Wang et al., 2015). Therefore, the bifacial gain also has a linear growth relationship under almost constant front irradiance when albedo increases (Gu et al., 2020; Yusufoglu et al., 2015), indicating that the bPV technology can take full advantage to generate more electricity in some places of high albedo (Wang et al., 2019). For example, the bifacial gain can reach 7.6%, 15.4% and 29.2% for ground having grass, sand and snow, respectively (Wei et al., 2016).

3.5.2 Tilt angle

Besides albedo, tilt angle also affects bPV performance greatly. The annual energy of the bPV and mPV modules is increased slightly until their optimal angles, respectively and then decreased sharply.

It is noted that the optimal angle of bPV modules is higher than the mPV under the same conditions (Patel et al., 2019; Sun et al., 2018). Tilt angle has less effect on the rear-side energy yield compared to the front-side. This is due to negligible effects on the diffuse and reflected irradiance from the sky and ground, demonstrating total bifacial energy yield and corresponding continuous increase in bifacial gain. High bifacial gain with large tilt angle can explain well the fact that vertical bPV technology is more recommended in some situations, such as the facade of a building and noise barriers.

3.5.3 *Elevation*

Elevation also affects the bifacial energy yield by affecting the rear irradiance (Yusufoglu et al., 2015). Due to more reflected irradiance from the ground and less self-shading, bifacial energy yield and bifacial gain, accelerate at high elevation, but with small growth rate (Deline et al., 2016; Kreinin et al., 2010). Therefore, usually it is suggested to set the elevation of the bPV modules as 0.5- 1.5 m above ground, to comprise electrical gain with the size of space (Gu et al., 2020; Yusufoglu et al., 2015).

3.5.4 *Orientation*

Bifacial PV performance greatly varies with the orientation as it affects the received irradiance (Sun et al., 2012). Fixed and tracking cases are considered, in order to accurately evaluate the effect of orientation. Both bPV and mPV modules with tracking technology produce more electricity than the fixed modules because of more irradiance. However, tracking technology does better to front-side

irradiance than the rear-side, resulting in lower bifacial gain with a tracking system. For the fixed case, the modules are installed facing south for higher energy yield. When facing east or west, the modules produce a little lower energy yield occurs but with higher bifacial gain, indicating that bPV technology is more flexible compared with the mPV, without the limits of orientation. It is noted that there are two peaks for the bPV power curve when the bPV module is vertical east-west-facing instead of the mPV module with one peak power as presented in Fig. 20 (Sun et al., 2018).

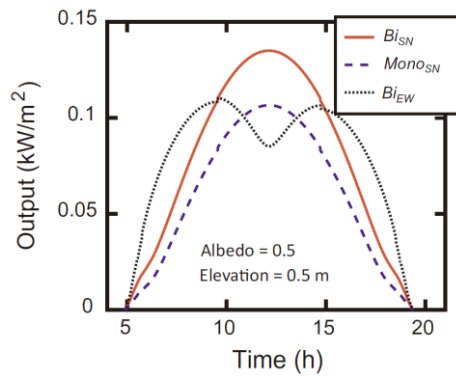


Fig. 20 PV power output of PV with different orientations ($Mono_{SN}$: south-north-facing mPV at optimal tilt angle; Bi_{SN} : south-north-facing bPV at optimal tilt angle; Bi_{EW} : vertical east-west-facing bPV) (Sun et al., 2018).

3.5.5 Row distance and row number

For more electricity production, many bPV modules are connected in series and parallels to form a bPV array. Under the circumstance, field installation (row distance and row number) becomes an indispensable factor of affecting the bPV performance (Lopez-Garcia et al., 2019; Pelaez et al., 2019).

According to the study of Shoukry et al. (Shoukry et al., 2016), bPV performance is better with larger

row spacing. When the distance between the module rows is fixed at 2.5 m, the bifacial gain for the PV modules in a PV array with 5×11 modules is presented in Fig. 21 (Shoukry et al., 2016). The performances of the modules at the edge and at the center of the field vary from 31.41% to 27.72%, which are obviously lower than a stand-alone bifacial module (33.85%).

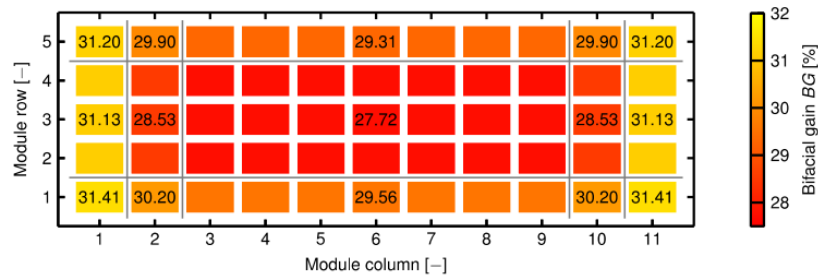


Fig. 21 Bifacial gain for a PV array with many rows (Shoukry et al., 2016).

3.5.6 Soiling and shading

It is obvious that soiling and shading have a negative effect on bifacial performance. To estimate the negative effect of soiling, the concepts of soiling loss in energy generation and soiling rate were employed by Bhaduri et al. (Bhaduri and Kottantharayil, 2019) and Luque et al. (Luque et al., 2018). Results show that vertical bPV modules have less soiling loss and average soiling rate. In addition, soiling loss of the bPV module is much lower than that of mPV in spite of front or rear side. Furthermore, a cleaning optimization model was developed to guide the cleaning strategy, suggesting that there is no need to clean the rear side because of less than 3% difference for cleaning as compared to not cleaning the rear-side.

For the shading effect, the bPV modules were validated by experiment to have 12.74% lower shading power loss rate than the mPV by affecting the fill factor (Bhang et al., 2019; Razongles et al., 2016). Moreover, the further behind the module and the whiter the shading objects are, lower the loss the bPV system suffers (De Groot and Van Aken, 2017), which suggests that it is better to place the white rocks further behind the PV module if it cannot be avoided.

In all, bPV technology has an advantage of suffering from less power loss due to soiling and shading under the same weather and installation conditions.

3.6 Test and characterization of the bPV modules

A standard test and characterization method is vital for bPV technology, which can provide manufacturers from different regions with a common approach to examine the bPV performance. Usually these test methods can be divided into two categories, namely indoor and outdoor.

3.6.1 Indoor performance characterization

As for bPV indoor performance characterization, it can be classified into single-side illumination and double-side illumination according to the number of light sources. For single-side illumination, front- and rear-side PV panels are characterized under 1000 W/m^2 separately, when the light from the opposite side is eliminated with a black rear cover placing at a distance from the PV panel as presented in Fig. 22 (a1)- (a3). Then, the power output can be regarded as an expression of equivalent irradiance,

which is also adopted in a technical specification, namely IEC TS 60904-1-2, published in 2019 (IEC, 2019).

For the equivalent irradiance, it can be expressed as Eq. (21):

$$G_{Ei} = G_f + \varphi G_{ri} \quad (21)$$

where G_{Ei} , G_f and G_{ri} are equivalent irradiance, front irradiance and rear irradiance of the bPV modules, and φ is the bifaciality, the minimum value between the bifaciality coefficients of short-circuit current and maximum power under STC, which can be calculated as:

$$\varphi = \text{Min}(\varphi_{I_{sc}}, \varphi_{P_{max}}) \quad (22)$$

$$\varphi_{I_{sc}} = \frac{I_{scr}}{I_{scf}} \quad (23)$$

$$\varphi_{P_{max}} = \frac{P_{maxr}}{P_{maxf}} \quad (24)$$

where $\varphi_{I_{sc}}$ and $\varphi_{P_{max}}$ is the bifaciality coefficients of short-circuit current and maximum power under STC, respectively, I_{scr} is the short-circuit current when the rear-side device is illuminated under STC, I_{scf} is the short-circuit current when the front-side device is illuminated under STC, P_{maxr} is the maximum power when the rear-side device is illuminated under STC, and P_{maxf} is the maximum power when the front-side device is illuminated under STC.

Therefore, two specific values of bPV power output, $P_{\text{max BiFi100}}$ and $P_{\text{max BiFi200}}$, can be calculated as

Eq. (25)- (26) under two reference irradiances ($G_{r1}= 100\text{W/m}^2$, $G_{r2}=200 \text{W/m}^2$):

$$P_{\max \text{ BiFi100}} = P_{\max \text{ STC}} + \text{BiFi} \cdot 100 \quad (25)$$

$$P_{\max \text{ BiFi200}} = P_{\max \text{ STC}} + \text{BiFi} \cdot 200 \quad (26)$$

where BiFi is rear irradiance driven power gain and $P_{\max \text{ STC}}$ is front-side power output of under STC.

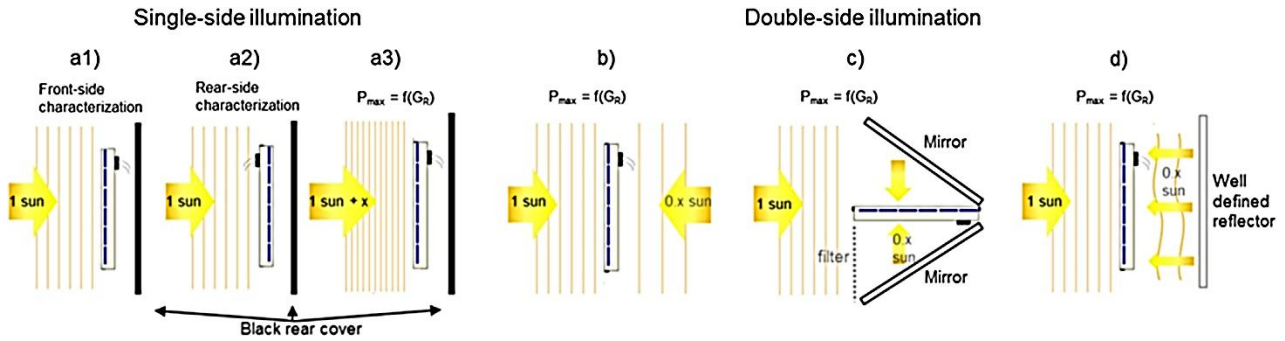


Fig. 22 Schematic measurement of indoor performance characterization: single-side illumination (a1, a2 and a3); double-side illumination (b, c and d) (Lopez-Garcia et al., 2019).

Another approach is double-side illumination based on the simultaneous illuminations of both sides with front irradiance at 1000 W/m^2 and at least two different rear irradiance. Apparently it is more straight but time-saving compared with single-side illumination, and different setups are employed during the testing process, such as two solar simulators (Fig. 22 b), tilted mirrors (Soria et al., 2016) (Fig. 22 c), and a well-defined reflector (Fig. 22 d), which also introduces some problems and challenges during the testing period (Liang, T. S. et al., 2018). For two solar simulators, timing of the two flashes simultaneously and controlling the reflected irradiance from the surroundings at the expense of additional solar simulator should be taken into consideration carefully. For the tilted mirror, only several rear-side irradiances can be set by filter instead of continuous irradiance level. For the

well-defined reflector, there are also many problems such as non-uniform rear irradiance, setting up specifications of the reflector material and distance from the bPV module (Lopez-Garcia et al., 2019).

3.6.2 Outdoor performance characterization

Similarly, it can also be classified into single-side illumination and double-side illumination for outdoor performance characterization of the bPV module. For single-side illumination, the concept of equivalent irradiance in section 3.6.1 is still valid during the tests as presented in Fig. 23 (a) where sunlight is the source of outdoor experiment. For double-side illumination, a reflective cloth or surfaces with a distance of 0.5-1 m from the bPV panel bottom are employed in order to change the ground albedo. At least two specific power values with different rear irradiances are also provided as Eq. (25)- (26). More details can also be found in the technical specification IEC TS 60904-1-2 (IEC, 2019).

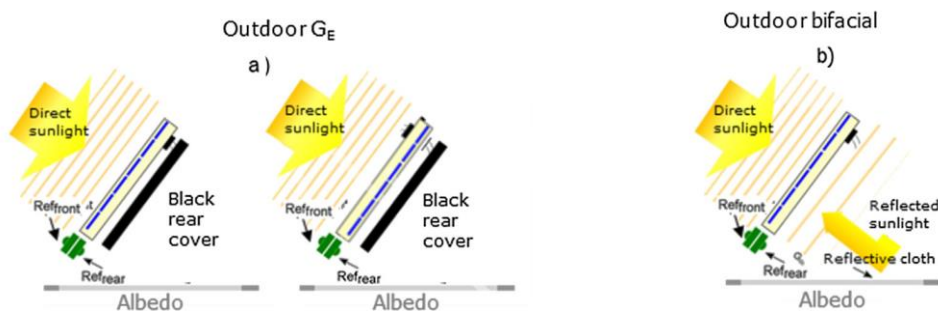


Fig. 23 Schematic measurement of outdoor performance characterization: a) single-side illumination; b) double-side illumination (Lopez-Garcia et al., 2019).

3.7 Practical applications

The bPV development can also be useful in other applications, including both space and terrestrial applications.

3.7.1 Space applications

The first space applications of bPV technology in the world could date from a space station named Salut-3 in 1974 (Bordina et al., 1976). Bifacial n^+p-p^+ contributed to a giant increase in electricity production, up to 34%, which led to the installation of bPV arrays on Salut-5 space station launched in 1976 (Eisenberg et al., 2008). Later, bPV arrays were installed on some satellites and famous spacecrafts (Prat et al., 1990), especially the bPV arrays on International Space Station (ISS), which consists of two American bPV arrays (December 2000), Russian “Zarya” (November 1998) and “Zvezda” (July 2000) Solar Arrays as presented in Fig. 24.

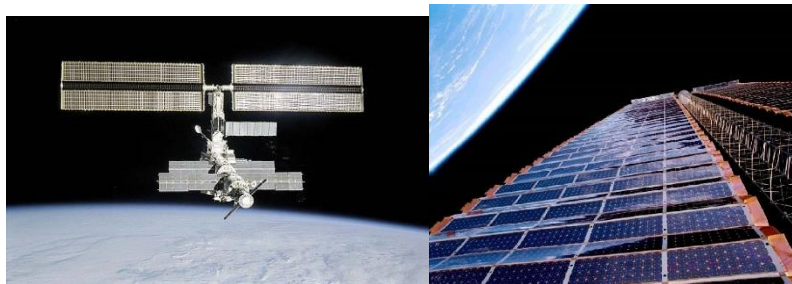


Fig. 24 The bPV modules on International Space Station (Delleur and Kerslake, 2002).

3.7.2 Terrestrial applications

3.7.2.1 Large-scale bPV plants

As lower LCOE is preferred by PV market, the utilizing sunlight from both sides, contributes to the development large-scale bPV plants. In 2013, the world's first large-scale bPV power station with installed capacity of 1.25 MW_p was set up and put into use in Hokuto City, Japan (Hokuto, 2013).

The PV plant showed huge electrical benefits and thus strengthened the confidence of investors persuading them to install more bPV plants around the world. Therefore, more and more large-scale PV plants with bPV technology were set up as presented in Table 2.

Table 2 Summary of global large-scale bPV plants (Chile, 2015; Datong, 2016; Dongying, 2018; Hokuto, 2013; Netherland, 2019; Traxscara, 2019; US, 2019; Wuhai, 2017).

Time	Location	Installed capacity (MW _p)	Module type, Manufacturer
2013	Hokuto City, Japan	1.25	EarthON 60 (EarthON cell), PVG Solutions
2015	Valparaiso, Chile	2.50	n-type BiSoN module (BiSoN cell), Megacell
2016	Datong City, Shanxi Province, China	50	n-type Panda module, Yingli Solar
2017	Wuhai City, Inner Mongolia Autonomous Region, China	100	n-type Panda module, Yingli Solar
2018	Dongying City, Shandong Province, China	100	PERC module, Almaden
2019	Netherlands	11.75	p-type module, Jolywood Solar
2019	Michel County, Georgia, USA	224	PERC module, LONGi Solar
2019	Traxscara, Mexico	220	p-type PERC, LONGi Solar

3.7.2.2 Building integrated with bPV

Besides the bPV plants, bPV technology is also employed into the building integrated photovoltaic (BIPV) field as a part of the building (Joge et al., 2003), such as vertical facade integration (Soria et al., 2016), shades (Hezel, 2003) and fences (Araki et al., 2009). There are numerous advantages to this application. Firstly, they not only generate electricity, but also function like conventional building materials. In addition, they remain clean and thus huge cleaning costs are reduced as they are less sensitive to snow, dust, etc. Moreover, orientation effect is not as strong as conventional mPV modules, meaning that they can face any orientation as designers demand, including east and west, an aspect that was very challenging in the past (Baumann et al., 2019).



Fig. 25 The applications of bPV modules in BIPV.

3.7.2.3 Noise barriers



Fig. 26 Applications of vertical bPV modules as noise barriers (Switzerland, 1997).

With increasing population and land price, there is not enough potential for PV installation with in cities. Under such conditions, vertical noise barriers (Fig. 26) are considered as an ideal solution to facilitate economy development and renewable energy supply (Faturrochman et al., 2018). Therefore, the first PV noise barriers were built in 1989 in Chur, Switzerland (Nordmann and Goetzberger, 1994), in which mPV modules were employed, followed by some other pilot installations (Faturrochman et al., 2018). Until 1997, the first bPV noise barriers in the world were installed and put into use in Switzerland (Switzerland, 1997). After these initial attempts, noise barriers with bigger capacities were built, for example, a bPV noise barrier of 730 kW_p was installed in Italy in 2009, and a series of bPV noise barriers ranging from 1 MW_p to 2.065 MW_p were installed in Germany (Faturrochman et al., 2018).

4 Outlook of bPV technology

As mentioned above, a lot of work has been done bPV development in areas of modelling, experiments and potential applications. However, there are still some challenges of modelling and performance estimations, which still require more research to move ahead. Therefore, in this section an outlook of the bPV technology is presented with some challenges and perspectives for future development.

4.1 Challenges of bPV technology

As the market of bPV technology increases rapidly, corresponding challenges have gradually emerged out, which hinder its widespread development.

4.1.1 Performance estimations

Unlike conventional energy sources, multi-physics processes are involved in bPV power generation. These include optical, electrical and thermal processes, which are tightly coupled, but rarely discussed in literature with relation to sunlight, electricity and heat. In addition, power output from the bPV modules is always expressed as a linear addition of front-side power under STC, and several particular rear-side irradiances from manufacturers (Gu et al., 2020). However, there is no linear relationship between bPV module power and irradiance, resulting in huge inaccuracy during power estimation, which should be carefully considered. Besides, electrical and thermal performance are always expressed by a simple equation, which cannot express the relationship between them. In fact, temperature distribution and power output are a function of environmental conditions (ambient temperature, wind velocity, solar radiation, and reflected radiation from ground). Moreover, solar irradiance especially reflected irradiance from ground is always associated with various installation conditions. Therefore, it is significant in the future to understand the relationships among them and then model their performance considering both simplification and accuracy.

Apart from modelling, long-term experiments should be conducted to evaluate the power output of bPV modules under real-world environment, instead of ideal conditions and unpractical assumptions, which may strongly affect the bPV performance.

4.1.2 Electrical mismatch

Electrical mismatch of bPV cells mainly result from uneven rear irradiance, as presented in Fig. 27 (De Groot and Van Aken, 2017). The highest rear irradiance of the PV cell (83 W/m^2) is 177% of the lowest rear irradiance (47 W/m^2). Such irradiance differences could result in uncertainty and reduction in power output by affecting the fill factor (Krein et al., 2010; Liang, T. S. et al., 2018). When these modules with inhomogeneous irradiance are connected in series and parallels to form a large-scale PV array, mismatch loss will contribute a great proportion in the whole system loss and thus need to be carefully controlled (Liang, Tian Shen et al., 2018; Lopez-Garcia et al., 2019). Therefore, the non-uniformity of less than 3 W/m^2 rear irradiance is highlighted several times in the technical specification IEC TS 60904-1-2 (IEC, 2019), which gradually becomes a huge challenge to face and solve in the PV field (Razongles et al., 2016). Therefore, despite various irradiance models being proposed, a suitable simplified and accurate model, especially for rear-side irradiance, which thus requires further research.

	A	B	C	D	E	F
1	65	64	63	63	63	62
2	75	74	73	74	75	77
3	72	70	69	69	68	72
4	66	65	65	66	68	70
5	53	50	47	49	52	57
6	54	51	49	51	52	56
7	53	54	55	56	58	61
8	62	59	56	58	59	63
9	66	61	56	59	61	66
10	72	67	62	65	69	75
11	79	78	76	77	78	79
12	76	73	70	73	77	83

Fig. 27 Measured rear-side irradiance of each cell in a bPV module (De Groot and Van Aken,

2017).

4.1.3 Systems optimization

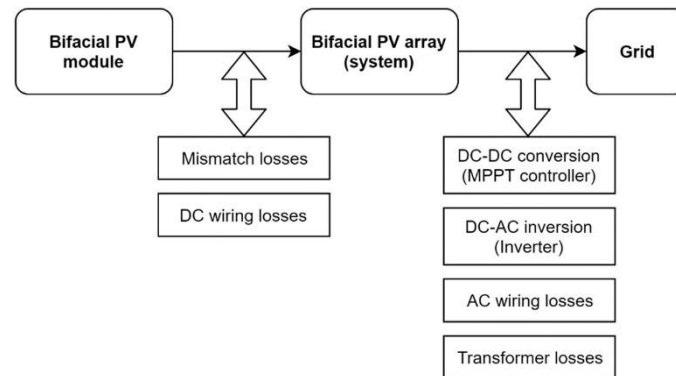


Fig. 28 Various system loss source for a bifacial system (Liang et al., 2019).

Besides bPV modules, components including inverters, MPPT and others should also be taken into consideration from manufacturing to installation to reduce the related energy loss for a specific bPV system as presented in Fig. 28 (Liang et al., 2019). DC wiring losses, DC-DC conversion, DC-AC inversion, AC wiring losses and transformer losses are some examples, which were rarely discussed in the past.

4.1.4 Economic and environmental estimations

The electrical performance of bPV modules has been discussed by many researchers from modelling or experiment. In contrast, there are few issues on economic and environmental estimations of bPV modules due to various reasons. On one hand, the value of electricity production is the foundation of the issues on economic and environmental estimations. However, there are still fierce arguments on how to calculate the power output of bPV modules, especially the power from the rear side of bPV modules. On the other hand, economic and environmental estimates especially LCOE are rather

complicated, because various factors also need to be taken into consideration in the financial model, such as the initial and maintenance costs.

4.2 Potential approaches and perspectives

The above challenges indicate that great efforts are needed to promote bPV technology. In this section, some potential approaches to optimize the bPV technology are discussed from the perspectives of cell, module and system, followed by some future perspectives.

4.2.1 Cost-effective cell designs

Cost-effective cell designs are crucial for better efficiency as some following methods describe:

- High power output of PV modules is always a top priority for companies. Larger cells are recommended because it can reduce the manufacturing cost of the cells and modules and corresponding costs on balance of system
- The half-cut cell technology cuts a standard-sized bPV cell by laser into two halves of the same size along a direction perpendicular to the busbars. This reduces the current of the half-cut cell, which ultimately improves bPV cell power output by 2%-4%. In addition, the half-cut cell exhibits excellent anti-blocking performance compared to conventional components due to its unique design, suitable for mounting the bPV cells on roofs.
- Multi-busbars (MBB) PV cells usually refer to the PV cells with over 6 busbars, and thinner solder ribbons for interconnection between the cells (Wohrle et al., 2017). This technology is

splendid in appearance and it can not only reduce manufacturing cost by saving over 50% silver paste in the bPV cell, but also increase the module power output through strong current collectivity and greater light receiving area. In addition, the power loss rate of the MBB bPV cells is still small, even when the cell sheet is cracked or chipped, which continuously maintains the power generation performance.

- The shingling technology is promising to further increase bifacial electrical density. An average electrical gain of 9.6% and 8% for 60-cell and 72-cell equivalent shingled modules (Tonini et al., 2018) is achieved, by cutting the whole solar cell into many pieces, and then overlapping each other with a selective Electrically Conductive Adhesive (ECA). Compared with mPV technology, this design is more compact and exhibits several advantages, such as low ohmic loss because of lower current (Tonini et al., 2018), high module power because of high package ratio, low residual cell stress and bowing due to low processing temperature of ECA (Beaucarne, 2016; Schulte-Huxel et al., 2019) and splendid aesthetics without visible busbars and ribbon soldering (Yagiura et al., 1997). However, more research needs to be done in order to optimize this novel technology, since it consists of issues like undeveloped equipment, lower module yield, high cost, patent breakthrough etc.

As the demand of cost-effective bPV modules increases, these novel cell designs combined with bPV technology will be used at a large scale in the near future.

4.2.2 Up conversion and down conversion

Novel methods with some specific structure to exceed the Shockley-Quisser limit for PV development are proposed, namely up conversion (UC) and down conversion (DC) (Green, 2006). Encapsulation structure of a bPV cell with UC is presented in Fig. 29 (Pan et al., 2014). UCs in silicone are attached to the back side of the industrial bPV cell. UC is a method of transmitting high-wavelengths (low-energy) photons from the solar spectrum to lower-wavelengths (high-energy) photons (Pan et al., 2016). Besides, PbS quantum dots (QDs) are employed in this study at the back side of the UCs layer due to their appropriate properties of absorption and emission. With the structure of UC and QDs, the absorption and efficiency are improved by reducing the reflection and transmittance as presented in Fig. 30. DC occurs when a specific material is used to absorb the photon at short wavelengths and emit it at long wavelengths. The material is always placed on the front side to reduce thermalization loss (Trupke et al., 2002). In all, UC and DC can be applied in bPV technology in the future to reduce transmission loss and thermalization loss for better efficiency of bPV modules.

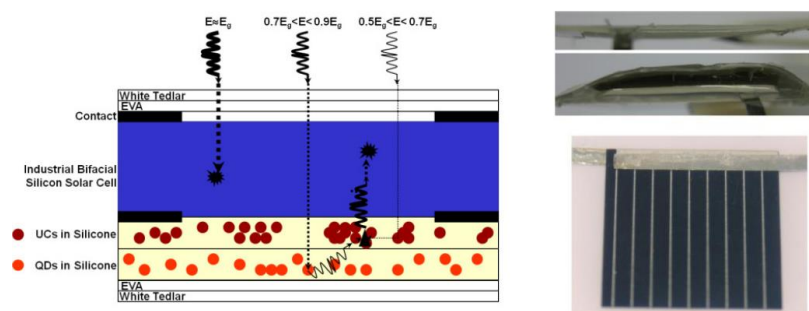


Fig. 29 Encapsulation structure of a bPV cell with UC and QDs (Pan et al., 2014).

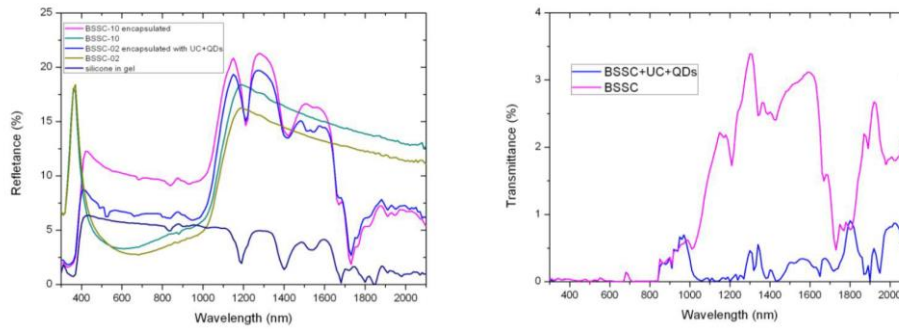


Fig. 30 Optical characterization of BSSC with and without UC and QDs (Pan et al., 2014).

4.2.3 Thermal management of bPV

The cell temperature of bifacial modules is higher than the mPV based on the literature (Lamers et al., 2018), the thermal management of bPV modules is a crucial aspect in the future.

Photovoltaic/thermal (PV/T) technology has the potential to spread from mPVs to bPVs, but this is met with some challenges, such as designing of the collector in a way that does not affect the irradiance of both sides. Fig. 31 presents two designs of bPV/T, namely air-cooling and water-cooling.

Four structures of air cooling are designed by Ooshaksaraei et al. (Ooshaksaraei et al., 2017), in which the energy efficiency of structure two is highest, followed by structure three, four, and one accordingly. For water cooling, 40% bifacial gain of bPV/T is achievable (Robles-Ocampo et al., 2007). However, these complex designs cannot obtain such obvious results, and even harm the electricity production due to lower received irradiance. Therefore, further in depth analysis on novel methods or materials, such as specific selective coolant and coating should be performed in the future for the development of bPV thermal management.

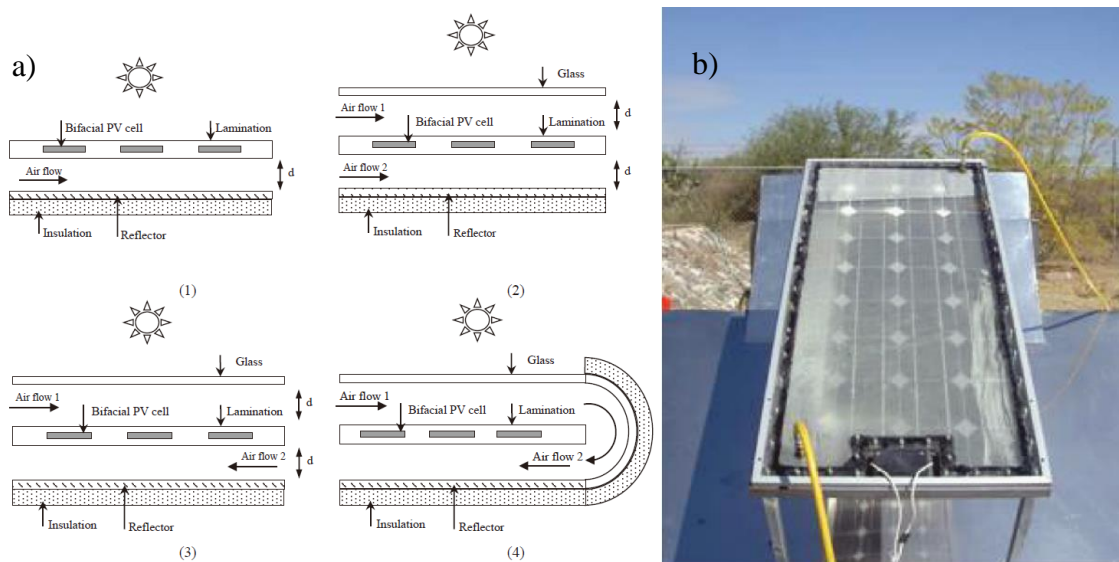


Fig. 31 Two types of bPV/T designs: a) air cooling (Ooshaksaraei et al., 2017); b) water cooling (Robles-Ocampo et al., 2007).

4.2.4 Solar tracking systems

As indicated above, different azimuthal angle means different irradiance on the plane of array due to changeable solar trace, which implies the potential of solar tracking systems combining with bPV technology (Al-Rousan et al., 2018). Obviously, these solar tracking systems have made use of the well-developed mPV technology in the past decade, especially various intelligent techniques (fuzzy logical, genetic algorithm etc.), while hardly making use of bPV technology. However, tracking systems will become widespread if combined with bPV technology as the attention of the market is shifted from mPV to bPV technology.

4.2.5 Revolution of module encapsulation

Tedlar and ethylene-vinyl acetate copolymer (EVA) are used as backsheet materials and cell encapsulation, when connecting many conventional PV cells in series to form a PV module. This will

not be suitable in the future for bPV module encapsulation as described in section 2.3.2 due to the many disadvantages under various conditions. Under such conditions, glass and ethylene-octene copolymer (POE) with low water vapor transmission rate and high volume resistivity are better choices to ensure a longer lifetime despite the glass backsheet's heavy weight. However, the industrial debate on whether to choose the structure of 'double glass' or 'glass-transparent organic materials' will be determined due to light weight and handy installation by the development of PV glass with thickness ≤ 2.0 mm in the future.

4.2.6 *Other future perspectives*

As above described, there are some other future perspectives for bPV technology from modeling, experiment and applications:

- In-depth research on multi-physics modelling is necessary to understand the relationship among sunlight, electricity and heat when designing and optimizing the bPV system. This should be carefully taken into consideration to estimate the electrical and thermal performance. Based on these performance indexes, especially power output, other economic and environmental indexes, such as LCOE and GPBT will be obtained accurately in the future.
- The performance of bPV modules is estimated by experiments under real-word environment, including fluctuating solar irradiance, ambient temperature and wind velocity. Therefore, more work should be conducted on evaluating the bPV performance through a long-term experiment.

- Some suggestions can be provided on loss mitigation and efficiency improvement. For instance, more module-scale MPPTs (micro inverters) are employed instead of string-level MPPTs (string inverter), and the uniform albedo and long row-to-row distance are beneficial to the uniform condition of rear irradiance. Additional similar approaches need to be further researched.
- Broad applications for bPV technology will be witnessed. For cities with high latitudes, more vertical bPV arrays will be widely used instead of mPV in the future, because of onsite weather and geographic features. For low-latitude cities, bPV modules will be recommended strongly if albedo is high, such as deserts. In addition, it may be a good choice to take hybrid deployments in bPV systems compromising economy with technical feasibility. For example, establishing mix of bPV modules facing east-west and mPV modules facing south in a bPV array.

5 Conclusions

The performance estimations and applications of bifacial photovoltaic (bPV) technology are hot topics in academia and PV markets. Many researchers have estimated the technical and economic performance of bPV technology by various models or experiments. Results show that the specific bifacial structure of bPV modules contributes to 5-30% more power output and 0-15.6% increase in initial cost, resulting in 2-6% lower levelized cost of energy (LCOE) than the mono-facial photovoltaic (mPV). To achieve high electricity production, all bPV modules should be installed in a tracking system at an optimal tilt angle with high albedo, elevation and row space. However, there are still some challenges as described above in practical applications. Especially the non-uniform

rear-side irradiance, which can result in electrical mismatch, receives increasing attention. Therefore, the simulation and measurement of non-uniform level is highlighted in bPV performance characterization methods in literature. Moreover, some potential approaches are proposed to make bPV technology more cost-effective from the optimization of cell, module and system, such as larger cell, up conversion and down conversion. Some future perspectives for bPV technology from modeling, experiment and applications as described above indicate that more research is still required for a wider spread of bPV technology in the future.

Acknowledgement

The authors would appreciate the financial supports provided by National Natural Science Foundation of China (NSFC) through the Grant 51976124.

References

- Abotaleb, A., Abdallah, A., 2018. Performance of bifacial-silicon heterojunction modules under desert environment. *Renewable Energy* 127, 94-101.
- Al-Rousan, N., Isa, N.A.M., Desa, M.K.M., 2018. Advances in solar photovoltaic tracking systems: A review. *Renewable and Sustainable Energy Reviews* 82, 2548-2569.
- Appelbaum, J., 2018. The role of view factors in solar photovoltaic fields. *Renewable and Sustainable Energy Reviews* 81, 161-171.

Araki, I., Tatsunokuchi, M., Nakahara, H., Tomita, T., 2009. Bifacial PV system in Aichi Airport-site Demonstrative Research Plant for New Energy Power Generation. *Solar Energy Materials and Solar Cells* 93(6-7), 911-916.

Asgharzadeh, A., Marion, B., Deline, C., Hansen, C., Stein, J.S., Toor, F., 2018. A Sensitivity Study of the Impact of Installation Parameters and System Configuration on the Performance of Bifacial PV Arrays. *IEEE Journal of Photovoltaics* 8(3), 798-805.

Bai, J., Liu, S., Hao, Y., Zhang, Z., Jiang, M., Zhang, Y., 2014. Development of a new compound method to extract the five parameters of PV modules. *Energy Conversion and Management* 79(2), 294-303.

Barbato, M., Barbato, A., Meneghini, M., Tavernaro, G., Rossetto, M., Meneghesso, G., 2017. Potential induced degradation of N-type bifacial silicon solar cells: An investigation based on electrical and optical measurements. *Solar Energy Materials and Solar Cells* 168, 51-61.

Baumann, T., Nussbaumer, H., Klenk, M., Dreisiebner, A., Carigiet, F., Baumgartner, F., 2019. Photovoltaic systems with vertically mounted bifacial PV modules in combination with green roofs. *Solar Energy* 190, 139-146.

Beaucarne, G., 2016. Materials Challenge for Shingled Cells Interconnection. *Energy Procedia* 98, 115-124.

Bhaduri, S., Kottantharayil, A., 2019. Mitigation of Soiling by Vertical Mounting of Bifacial Modules. *IEEE Journal of Photovoltaics* 9(1), 240-244.

Bhang, B.G., Lee, W., Kim, G.G., Choi, J.H., Park, S.Y., Ahn, H.-K., 2019. Power Performance of Bifacial c-Si PV Modules With Different Shading Ratios. *IEEE Journal of Photovoltaics*, 1-8.

Bordina, N.M., Borisova, N.A., Daletskii, G.S., Zadde, V.V., Zaitseva, A.K., Landsman, A.P., Letin, V.A., 1976. Using the radiation reflected from the earth for increasing the power of solar batteries. *Cosmic Res* 14(2), 266-272.

Branker, K., Pathak, M.J.M., Pearce, J.M., 2011. A review of solar photovoltaic levelized cost of electricity. *Renewable and Sustainable Energy Reviews* 15(9), 4470-4482.

Carolus, J., Tsanakas, J.A., van der Heide, A., Voroshazi, E., De Ceuninck, W., Daenen, M., 2019. Physics of potential-induced degradation in bifacial p-PERC solar cells. *Solar Energy Materials and Solar Cells* 200.

Castillo-Aguilella, J.E., Hauser, P.S., 2016. Multi-Variable Bifacial Photovoltaic Module Test Results and Best-Fit Annual Bifacial Energy Yield Model. *IEEE Access* 4, 498-506.

Chen, Z., Chen, Y., Wu, L., Cheng, S., Lin, P., You, L., 2019. Accurate modeling of photovoltaic modules using a 1-D deep residual network based on I-V characteristics. *Energy Conversion and Management* 186, 168-187.

Chile, 2015. World's largest bifacial PV plant nears completion in Chile.

Comsol, 2014. Simulate Ray Tracing in Optically Large Systems with the Ray Optics Module.

Cuevas, A., Luque, A., Eguren, J., del Alamo, J., 1982. 50 Percent more output power from an albedo-collecting flat panel using bifacial solar cells. *Solar Energy* 29(5), 419-420.

Datong, 2016. Yingli Green completes 50MW 'Top Runner' PV power plant project. Available: <http://www.pv-tech.cn/news/yingli-green-completes-50mw-top-runner-pv-power-plant-project>;

De Groot, K.M., Van Aken, B.B., 2017. Near-field partial shading on rear side of bifacial modules. *Energy Procedia* 124, 532-539.

Deline, C., MacAlpine, S., Marion, B., Toor, F., Asgharzadeh, A., Stein, J.S., 2016. Evaluation and field assessment of bifacial photovoltaic module power rating methodologies, 2016 IEEE 43rd Photovoltaic Specialists Conference (PVSC). pp. 3698-3703.

Deline, C., Pel áez, S.A., Marion, B., Sekulic, B., Woodhouse, M., Stein, J., 2019. Bifacial PV System Performance: Separating Fact from Fiction. Plenary presentation at Photovoltaics Specialists Conference.

Delleur, A.M., Kerslake, T.W., 2002. Electrical performance of the international space station US photovoltaic array during bifacial illumination, IECEC'02. 2002 37th Intersociety Energy Conversion Engineering Conference, 2002. IEEE, pp. 39-44.

Dobos, A.P., 2012. An improved coefficient calculator for the california energy commission 6 parameter photovoltaic module model. *Journal of Solar Energy Engineering, Transactions of the ASME* 134(2).

Dongying, 2018. China's first and largest double-sided double-glass component power plant project is about to be connected to the grid.

Duffie, J.A., Beckman, W.A., Worek, W.M., 2006. *Solar Engineering of Thermal Process*. A Wiley-Interscience Publication 116(1), 549.

- Eisenberg, N., Bordin, N., Kreinin, L., Kalikauskas, V.S., Zviagina, K.N., Kagan, M., Grigorieva, G., 2008. Future of Bifacial Si Solar Cells for Space Applications. 23rd European Photovoltaic Solar Energy Conference and Exhibition.
- Faiman, D., 2008. Assessing the outdoor operating temperature of photovoltaic modules. *Progress in Photovoltaics: Research and Applications* 16(4), 307-315.
- Faturrochman, G.J., de Jong, M.M., Santbergen, R., Folkerts, W., Zeman, M., Smets, A.H.M., 2018. Maximizing annual yield of bifacial photovoltaic noise barriers. *Solar Energy* 162, 300-305.
- Fertig, F., Nold, S., Währle, N., Greulich, J., Hädrich, I., Krauß, K., Mittag, M., Biro, D., Rein, S., Preu, R., 2016. Economic feasibility of bifacial silicon solar cells. *Progress in Photovoltaics: Research and Applications* 24(6), 800-817.
- Green, M.A., 2006. *Third Generation Photovoltaics: Advanced Solar Energy Conversion*.
- Gu, W., Ma, T., Li, M., Shen, L., Zhang, Y., 2020. A coupled optical-electrical-thermal model of the bifacial photovoltaic module. *Applied Energy* 258, 114075.
- Gu, W., Ma, T., Shen, L., Li, M., Zhang, Y., Zhang, W., 2019a. Coupled electrical-thermal modelling of photovoltaic modules under dynamic conditions. *Energy* 188.
- Gu, W., Ma, T., Song, A., Li, M., Shen, L., 2019b. Mathematical modelling and performance evaluation of a hybrid photovoltaic-thermoelectric system. *Energy Conversion and Management* 198.
- Guerrero-Lemus, R., Vega, R., Kim, T., Kimm, A., Shephard, L.E., 2016. Bifacial solar photovoltaics – A technology review. *Renewable and Sustainable Energy Reviews* 60, 1533-1549.

Guo, S., Walsh, T.M., Peters, M., 2013. Vertically mounted bifacial photovoltaic modules: A global analysis. *Energy* 61, 447-454.

Hezel, R., 2003. Novel applications of bifacial solar cells. *Progress in Photovoltaics: Research and Applications* 11(8), 549-556.

Hiroshi, M., 1966. Radiation energy transducing device. US Patent.

Hokuto, 2013. Japan's Asahikawa megawatt-scale photovoltaic power station: using double-sided light-receiving panels to "turn snow into treasure". Available: <<http://www.ne21.com/news/show-51711.html>>.

Humada, A.M., Hojabri, M., Mekhilef, S., Hamada, H.M., 2016. Solar cell parameters extraction based on single and double-diode models: A review. *Renewable and Sustainable Energy Reviews* 56, 494-509.

IEC, 2019. IEC TS 60904-1-2. Available: <<https://webstore.iec.ch/publication/34357>>.

Joge, T., Araki, I., Takaku, K., Nakahara, H., Eguchi, Y., Tomita, T., 2003. Advanced applications of bifacial solar modules. *3rd World Conference on Photovoltaic Energy Conversion* 3, 2451-2454.

Kasahara, N., Yoshioka, K., Saitoh, T., 2003. Performance evaluation of bifacial photovoltaic modules for urban application. *World Conference on Photovoltaic Energy Conversion*, 2455-2458.

Katsaounis, T., Kotsovos, K., Gereige, I., Basaheeh, A., Abdullah, M., Khayat, A., Al-Habshi, E., Al-Saggaf, A., Tzavaras, A.E., 2019. Performance assessment of bifacial c-Si PV modules through device simulations and outdoor measurements. *Renewable Energy* 143, 1285-1298.

Kreinin, L., Bordin, N., Karsenty, A., Drori, A., Grobgeld, D., Eisenberg, N., 2010. PV module power gain due to bifacial design. Preliminary experimental and simulation data. 2010 35th IEEE Photovoltaic Specialists Conference, 002171-002175.

Kutzer, M., Fülle, A., Jahnke, A., Becker, J., Hahn, H., Wendt, S., Witzig, A., Stöckli, U., Neuhaus, D., Kunath, L., 2016. Ertragssteigerung durch bifaciale Modultechnologie.

Lamers, M.W.P.E., Özkalay, E., Gali, R.S.R., Janssen, G.J.M., Weeber, A.W., Romijn, I.G., Van Aken, B.B., 2018. Temperature effects of bifacial modules: Hotter or cooler? *Solar Energy Materials and Solar Cells* 185, 192-197.

LBNL, 1990s. RADIANCE software.

Liang, T.S., Poh, D., Pravettoni, M., 2018. Challenges in the pre-normative characterization of bifacial photovoltaic modules. *Proceedings of the 12th International Photovoltaic Power Generation and Smart Energy Conference & Exhibition (Snec2018)* 150, 66-73.

Liang, T.S., Poh, D., Pravettoni, M., 2018. Challenges in the pre-normative characterization of bifacial photovoltaic modules. *Energy Procedia* 150, 66-73.

Liang, T.S., Pravettoni, M., Deline, C., Stein, J.S., Kopecek, R., Singh, J.P., Luo, W., Wang, Y., Aberle, A.G., Khoo, Y.S., 2019. A review of crystalline silicon bifacial photovoltaic performance characterisation and simulation. *Energy & Environmental Science* 12(1), 116-148.

Liu, B.Y.H., Jordan, R.C., 1963. The long-term average performance of flat-plate solar-energy collectors: With design data for the U.S., its outlying possessions and Canada. *Solar Energy* 7(2), 53-74.

Lopez-Garcia, J., Casado, A., Sample, T., 2019. Electrical performance of bifacial silicon PV modules under different indoor mounting configurations affecting the rear reflected irradiance. *Solar Energy* 177, 471-482.

LRC, 2020. TracePro software.

Luque, A., Ruiz, J., Cuevas, A., Eguren, J., Agost, M., 1978. Double Sided (D. S.) Solar Cells to Improve Static Concentration. *Photovolt. Sol. Energy Conf.*

Luque, E.G., Antonanzas-Torres, F., Escobar, R., 2018. Effect of soiling in bifacial PV modules and cleaning schedule optimization. *Energy Conversion and Management* 174, 615-625.

Ma, T., Zhao, J., Li, Z., 2018. Mathematical modelling and sensitivity analysis of solar photovoltaic panel integrated with phase change material. *Applied Energy* 228, 1147-1158.

Mermoud, A., Wittemer, B., 2018. Yield Simulations for Horizontal Axis Trackers with Bifacial PV Modules in PVsyst, 35th European Photovoltaic Solar Energy Conference.

Merten, J., Andreu, J., 1998. Clear separation of seasonal effects on the performance of amorphous silicon solar modules by outdoor I/V-measurements. *Solar Energy Materials & Solar Cells* 52(1-2), 11-25.

Merten, J., Asensi, J.M., Voz, C., Shah, A.V., Platz, R., Andreu, J., 1998. Improved equivalent circuit and analytical model for amorphous silicon solar cells and modules. *IEEE Transactions on Electron Devices* 45(2), 423-429.

Merten, J., Coignus, J., Razongles, G., Muñoz, D., 2012. Novel Equivalent Circuit for Heterojunction Cells and Diagnostic Method Based on Variable Illumination Measurements (VIM).

Merten, J., Sicot, L., Delesse, Y., Montgareuil, A.G.D., 2008. Outdoor evaluation of the energy production of different module technologies. 23rd EU-PVSEC.

Molin, E., Stridh, B., Molin, A., Wackelgard, E., 2018. Experimental Yield Study of Bifacial PV Modules in Nordic Conditions. IEEE Journal of Photovoltaics 8(6), 1457-1463.

Netherland, 2019. A major breakthrough! Europe's largest N-type double-sided solar power plant successfully connected to the grid.

Nordmann, T., Goetzberger, A., 1994. Motorway sound barriers: recent results and new concepts for advancement of technology.

NREL, Bifacialvf - Bifacial PV View Factor model. Available: <https://github.com/NREL/bifacialvf>.

NREL, 2018a. PVSyst software v 6.78. Available: <https://www.pvsyst.com/download-pvsyst/>.

NREL, 2018b. SAM 2018.11.11 for Windows. Available: <https://sam.nrel.gov/download.html>.

Ooshaksaraei, P., Sopian, K., Zaidi, S.H., Zulkifli, R., 2017. Performance of four air-based photovoltaic thermal collectors configurations with bifacial solar cells. Renewable Energy 102, 279-293.

Pan, A.C., Cardoso, L.S.G., Reis, F.S.d., 2016. Modeling Mathematical of the Behavior of Up Converter when Implemented in Bifacial Silicon Solar Cells. Energy Procedia 102, 80-86.

Pan, A.C., Zanesco, I., Moehlecke, A., 2014. Industrial Bifacial Silicon Solar Cells with Up-converter and PbS Quantum Dots. Energy Procedia 44, 160-166.

Pan, Z., Bi, Y., An, L., 2020. A cost-effective and chemically stable electrode binder for alkaline-acid direct ethylene glycol fuel cells. *Applied Energy* 258.

Patel, M.T., Khan, M.R., Sun, X., Alam, M.A., 2019. A worldwide cost-based design and optimization of tilted bifacial solar farms. *Applied Energy* 247, 467-479.

Pelaez, S.A., Deline, C., MacAlpine, S.M., Marion, B., Stein, J.S., Kostuk, R.K., 2019. Comparison of Bifacial Solar Irradiance Model Predictions With Field Validation. *Ieee Journal of Photovoltaics* 9(1), 82-88.

Perez, R., Stewart, R., Arbogast, C., Seals, R., Scott, J., 1986. An anisotropic hourly diffuse radiation model for sloping surfaces: Description, performance validation, site dependency evaluation. *Solar Energy* 36(6), 481-497.

Piccoli, E., 2017. Modeling an innovate shading device integrating PV. *Universitat Politècnica de Catalunya*.

Prat, L., Alcubilla, R., Blasco, E., Garcia, E., Calderer, J., Correig, X., Castañer, L., 1990. Performance analysis of bifacial silicon solar cells in a space environment. *Solar Cells* 29(4), 303-318.

Rabanal-Arabach, J., Schneider, A., 2016. Anti-reflective Coated Glass and its Impact on Bifacial Modules' Temperature in Desert Locations. *Energy Procedia* 92, 590-599.

Razongles, G., Sicot, L., Joanny, M., Gerritsen, E., Lefillastre, P., Schroder, S., Lay, P., 2016. Bifacial Photovoltaic Modules: Measurement Challenges. *Energy Procedia* 92, 188-198.

REN21, Renewables 2019 Global Status Report. Available: <<http://www.ren21.net/gsr-2019/pages/foreword/foreword/>>.

Robles-Ocampo, B., Ruíz-Vasquez, E., Canseco-Sánchez, H., Cornejo-Meza, R.C., Trápaga-Martínez, G., García-Rodríguez, F.J., González-Hernández, J., Vorobiev, Y.V., 2007.

Photovoltaic/thermal solar hybrid system with bifacial PV module and transparent plane collector.

Solar Energy Materials and Solar Cells 91(20), 1966-1971.

Rodríguez-Gallegos, C.D., Bieri, M., Gandhi, O., Singh, J.P., Reindl, T., Panda, S.K., 2018.

Monofacial vs bifacial Si-based PV modules: Which one is more cost-effective? Solar Energy 176, 412-438.

Sandia, Sandia National Laboratories. Field Example of Bifacial Gain at Sandia.

Sandia, Sandia National Laboratories. PV_LIB Toolbox. Available: <https://pvpmc.sandia.gov/applications/pv_lib-toolbox/>.

Sandia, Sandia National Laboratories. Sandia Cell Temperature Model.

Sandia, Sandia National Laboratories. Sandia Module Temperature Model.

Saw, M.H., Khoo, Y.S., Singh, J.P., Wang, Y., 2017. Enhancing optical performance of bifacial PV modules. 7th International Conference on Silicon Photovoltaics, Siliconpv 2017 124, 484-494.

Schulte-Huxel, H., Blankemeyer, S., Morlier, A., Brendel, R., Köntges, M., 2019. Interconnecting shingling: Maximizing the active module area with conventional module processes. Solar Energy Materials and Solar Cells 200, 109991.

Shoukry, I., Libal, J., Kopecek, R., Wefringhaus, E., Werner, J., 2016. Modelling of Bifacial Gain for Stand-alone and in-field Installed Bifacial PV Modules. Energy Procedia 92, 600-608.

Singh, J.P., Guo, S., Peters, I.M., Aberle, A.G., Walsh, T.M., 2015. Comparison of Glass/Glass and Glass/Backsheet PV Modules Using Bifacial Silicon Solar Cells. IEEE Journal of Photovoltaics 5(3), 783-791.

Solargis, SolarGIS: Solar resource maps and GIS data for 200+ countries. Available: <<https://solargis.com/maps-and-gis-data/overview>>.

Sönmez, F.F., Ziar, H., Isabella, O., Zeman, M., 2019. Fast and accurate ray-casting-based view factor estimation method for complex geometries. Solar Energy Materials and Solar Cells 200.

Soria, B., Gerritsen, E., Lefillastre, P., Broquin, J.-E., 2016. A study of the annual performance of bifacial photovoltaic modules in the case of vertical facade integration. Energy Science & Engineering 4(1), 52-68.

Sporleder, K., Naumann, V., Bauer, J., Richter, S., Hähnel, A., Großer, S., Turek, M., Hagendorf, C., 2019. Root cause analysis on corrosive potential-induced degradation effects at the rear side of bifacial silicon PERC solar cells. Solar Energy Materials and Solar Cells 201.

Stein, J.S., Hansen, C.W., Reno, M.J., 2012. Global Horizontal Irradiance Clear Sky Models: Implementation and Analysis. SANDIA REPORT.

Stein, J.S., Riley, D., Lave, M., Hansen, C., Deline, C., Toor, F., 2017. Outdoor Field Performance from Bifacial Photovoltaic Modules and Systems. 2017 Ieee 44th Photovoltaic Specialist Conference (PVSC), 3184-3189.

Sun, L., Lu, L., Yang, H., 2012. Optimum design of shading-type building-integrated photovoltaic claddings with different surface azimuth angles. *Applied Energy* 90, 233-240.

Sun, X., Khan, M.R., Deline, C., Alam, M.A., 2018. Optimization and performance of bifacial solar modules: A global perspective. *Applied Energy* 212, 1601-1610.

Switzerland, 1997. World's first bifacial sound insulation system near Wallisellen / Zurich, 10 kWp pilot system.

Tillmann, P., Jäger, K., Becker, C., 2020. Minimising the levelised cost of electricity for bifacial solar panel arrays using Bayesian optimisation. *Sustainable Energy & Fuels* 4(1), 254-264.

Tonini, D., Cellere, G., Bertazzo, M., Fecchio, A., Cerasti, L., Galiazzo, M., 2018. Shingling Technology For Cell Interconnection: Technological Aspects And Process Integration. *Energy Procedia* 150, 36-43.

Tossa, A.K., Soro, Y.M., Azoumah, Y., Yamegueu, D., 2014. A new approach to estimate the performance and energy productivity of photovoltaic modules in real operating conditions. *Solar Energy* 110, 543-560.

Traxscara, 2019. Mexico's largest bifacial photovoltaic power station.

Trupke, T., Green, M.A., Würfel, P., 2002. Improving solar cell efficiencies by down-conversion of high-energy photons. *Journal of Applied Physics* 92(3), 1668-1674.

US, 2019. LONGi will supply 224MW double-sided PERC components for the largest "double-sided + tracking" project in the US.

Van Aken, B.B., Carr, A.J., 2014. Relating Indoor and Outdoor Performance of Bifacial Modules. 2014 Ieee 40th Photovoltaic Specialist Conference (Pvsc), 1381-1383.

VDMA, 2019. International Technology Roadmap for Photovoltaic (ITRPV). Available: <<https://itrpv.vdma.org/en/>>.

Wang, L., Liu, F., Yu, S., Quan, P., Zhang, Z., 2019. The Study on Micromismatch Losses of the Bifacial PV Modules Due to the Irradiance Nonuniformity on Its Backside Surface. IEEE Journal of Photovoltaics, 1-9.

Wang, S., Wilkie, O., Lam, J., Steeman, R., Zhang, W., Khoo, K.S., Siong, S.C., Rostan, H., 2015. Bifacial Photovoltaic Systems Energy Yield Modelling. Energy Procedia 77, 428-433.

Wei, Q., Wu, C., Liu, X., Zhang, S., Qian, F., Lu, J., Lian, W., Ni, P., 2016. The Glass-glass Module Using n-type Bifacial Solar Cell with PERT Structure and its Performance. Energy Procedia 92, 750-754.

Wohrle, N., Fellmeth, T., Greulich, J., Bitnar, B., Neuhaus, H., Palinginis, P., Kohler, R., Rein, S., 2017. Understanding the rear-side layout of p-doped bifacial PERC solar cells with simulation driven experiments. 7th International Conference on Silicon Photovoltaics, Siliconpv 2017 124, 225-234.

Wuhai, 2017. Yingli Green using bifacial modules in 100MW 'Top Runner' project.

Yagiura, T., Morizane, M., Murata, K., Uchihashi, K., Tsuda, S., Nakano, S., Ito, T., Omoto, S.,

Yamashita, Y., Yamakawa, H., Fujiwara, T., 1997. Exchangeable PV shingle. Solar Energy Materials and Solar Cells 47(1), 227-233.

Yordanov, G.H., Midtgård, O.-M., Saetre, T.O., 2012. Series resistance determination and further characterization of c-Si PV modules. *Renewable Energy* 46(5), 72-80.

Yu, B., Song, D., Sun, Z., Liu, K., Zhang, Y., Rong, D., Liu, L., 2016. A study on electrical performance of N-type bifacial PV modules. *Solar Energy* 137, 129-133.

Yusufoglu, U.A., Lee, T.H., Pletzer, T.M., Halm, A., Koduvelikulathu, L.J., Comparotto, C., Kopecek, R., Kurz, H., 2014. Simulation of Energy Production by Bifacial Modules with Revision of Ground Reflection. *Energy Procedia* 55, 389-395.

Yusufoglu, U.A., Pletzer, T.M., Koduvelikulathu, L.J., Comparotto, C., Kopecek, R., Kurz, H., 2015. Analysis of the Annual Performance of Bifacial Modules and Optimization Methods. *IEEE Journal of Photovoltaics* 5(1), 320-328.